

# Prequel to the Stories of Warm Conveyor Belts and Atmospheric Rivers

The Moist Tongues Identified by Rossby and His Collaborators in the 1930s

Ruping Mo

**ABSTRACT:** The model of atmospheric rivers (ARs) has been around since the 1990s. A closely related model is the warm conveyor belt (WCB) developed in the 1970s. Looking further back in time, a phenomenon known as the “moist tongue” was intensively investigated in the late 1930s and early 1940s by Rossby and his collaborators using the innovation of isentropic analysis. This article aims to establish a historical perspective on the development of the moist tongue model and its relevance to the current models of WCBs and ARs. As it turns out, the moist tongue was identified as an extension of moist air into a region of lower moisture content on the selected isentropic charts. Most moist tongues are driven by large-scale cyclonic and anticyclonic eddies and are often accompanied by surface cold fronts in close proximity. Ahead of the moist tongues, areas of continuous precipitation are caused mainly by the motion of moist air up the steep isentropic slopes over warm fronts or topographical features. In the warm season, the mere presence of a moist tongue could be sufficient to give thunderstorms. A reanalysis dataset is used to reexamine the structures and evolutions of two moist tongue events in 1936. It is shown that not all but some of the moist tongues fit well with the modern conceptual models of WCB and AR. These two case studies also serve to elucidate the usefulness of reanalysis data for investigating historical high-impact weather events that were poorly understood due to the lack of observational data.

**KEYWORDS:** Extratropical cyclones; Atmospheric river; Jets; Synoptic-scale processes; Isotopic analysis; Forecasting techniques

<https://doi.org/10.1175/BAMS-D-20-0276.1>

Corresponding author: Dr. R. Mo, [ruping.mo@ec.gc.ca](mailto:ruping.mo@ec.gc.ca)

In final form 30 December 2021

For information regarding reuse of this content and general copyright information, consult the [AMS Copyright Policy](#).

**T**he atmospheric river (AR) phenomenon has been the subject of intensive research and applications in recent decades (Gimeno et al. 2014; Ralph et al. 2017a, 2018, 2020). This synoptic-scale system can be generally defined as a long ( $\geq 2,000$  km), narrow ( $\leq 1,000$  km), and transient corridor of strong horizontal water vapor transport concentrated in the lower troposphere (Zhu and Newell 1998; Ralph et al. 2004). It is typically associated with a low-level jet (LLJ) ahead of the cold front of an extratropical cyclone, and its landfall over mountainous terrain has the potential to produce extreme precipitation and severe flooding. The aim of this article is to build a bridge between the contemporary notion of ARs and the concept of the moist tongue introduced by Carl-Gustaf Rossby and his colleagues in the 1930s (Rossby et al. 1937a,b). While the main motivation of Rossby's team was to promote isentropic analysis and show evidence of large-scale mixing in the atmosphere, their studies also showed how isentropic charts could be used to trace the moisture from its source to the areas of condensation and precipitation (Byers 1960).

The terminology of AR was conceived and developed in the early 1990s. In a pilot study, Newell et al. (1992) showed that a filamentary structure is a common feature of water vapor transport in the troposphere. They called these filaments “tropospheric rivers” because some may carry as much water as the Amazon. This term was soon renamed as AR by Zhu and Newell (1994); also see Espenak and Anderson (1993, p. 12). Newell et al. (1992) noticed that filamentary cloud bands had been documented and discussed earlier, but the associated moisture fluxes had not been calculated (e.g., McGuirk et al. 1987; Kuhnel 1989). These cloud bands were known as “tropical plumes” (TP) in the 1990s (McGuirk et al. 1988; McGuirk and Ulsh 1990; Iskenderian 1995). It was also in the 1990s when “pineapple express” (PE) emerged as a popular term in both media and academia to describe an LLJ in the northeastern Pacific that brings warm, moist air from the area around Hawaii to the west coast of North America (Pryne and Long 1991; Waters 1993; Davis 1995; Loukas and Quick 1996; Wood 1998; Lackmann and Gyakum 1999). The combined effect of the moist LLJ and orographic uplift can cause some extremely heavy rainstorms in western North America (Dettinger 2004; Conrad 2009; Mo 2016). A typical example is the landfall of a PE storm during 13–15 November 2021 that triggered one of the most destructive and expensive weather disasters in Canadian history. For just over two days, massive amounts of rain (200–300 mm in some places with melting snow in high terrain) swamped the already soggy south coast and interior of British Columbia, leading to widespread floods, mudslides, debris flows, and highway washouts; this perfect storm caused the loss of at least 6 lives and close to 15,000 evacuations (Environment and Climate Change Canada 2021). Note that both PE and TP storms were referred to as “tropical moisture export” (TME) events by Knippertz and Wernli (2010).

The first milestone for the AR theory was set by Zhu and Newell (1998), who published an algorithm for AR identification and showed that ARs are responsible for most of the meridional moisture transport in the extratropical atmosphere. Their result indicates that ARs can play a critical role in shaping global water and energy cycles, and their algorithm can be used to track ARs on a daily basis in operational forecasting. Up to this time the river analogy had not been widely recognized (Davis et al. 1993; Eerme 1996; Katzfey and McInnes 1996; Iselin and Gutowski 1997; Wernli and Davies 1997), and there was concern that the

definition of “rivers” is based purely upon an Eulerian analysis, while the term implies a Lagrangian character (Wernli 1997). It was not until the publications of Ralph et al. (2004) that the AR notion was widely accepted and appreciated in the scientific communities (e.g., Smirnov and Moore 1999, 2001; Gyakum 2000; James and Houze 2005; Ralph et al. 2005, 2006; Kerr 2006; Jankov et al. 2007; Neiman et al. 2008a,b; Kaplan et al. 2009; Guan et al. 2010; Lavers et al. 2011, 2012; Sodemann and Stohl 2013; Gorodetskaya et al. 2014; Dacre et al. 2015; Gimeno et al. 2016; Paltan et al. 2017; Zhou et al. 2018; Mo et al. 2019, 2021; Tan et al. 2020; Ye et al. 2020; Black et al. 2021; Fu et al. 2021). The conceptual model in Ralph et al. (2004) not only portrays the AR as a pre-cold-frontal moisture conveyor belt, but also emphasizes its capability to produce extreme precipitation and form a critical link between weather and climate (also see Ralph et al. 2017b).

The location of the AR along an LLJ within the warm sector of a midlatitude cyclone shares kinematic and thermodynamic properties of a system called the warm conveyor belt (WCB), which was recognized in the 1970s as a narrow airstream transporting large amounts of heat, moisture, and westerly momentum (Browning 1971; Browning and Pardoe 1973; Harrold 1973). The conceptual model of the WCB depicts a tongue of moist and warm air flowing ahead of the cold front and ascending in the warm sector as it approaches the warm front associated with a cyclone; the WCB favors heavy precipitation along the isentropes closer to the warm front and cyclone center, where moist air rises more rapidly to achieve saturation before joining the upper-level westerly flow (Carlson 1980; Browning 1986, 1990). The occurrence of heavy precipitation ahead of the cold front may also be favored when the WCB environment provides a potential source for instability in conjunction with lift provided by the cold front. The warm, moist air flowing along the length of the cold front is what we call the AR today. It has been suggested that “moisture conveyor belt” could be a better term than AR to represent strong moisture transport because it is more consistent with the well-established WCB model (e.g., Bao et al. 2006; Knippertz and Martin 2007). To set the stage for a global science of ARs, a workshop held in 2015 brought together experts on ARs, WCBs, and TMEs to discuss the relationships among these interrelated concepts; the group reached consensus on redefining the WCB as a zone of dynamically uplifted heat and water vapor transport close to an extratropical cyclone, the TME as a zone of intense moisture transport out of the tropics, and the AR as a low-level corridor of strong moisture transport that often connects a TME to a WCB or an orographically induced rainout (Dettinger et al. 2015; Ralph et al. 2018).

Dating further back in time, we encounter the “moist tongue” (MT) and “dry tongue” (DT) coined by Rossby et al. (1937a,b). The MT was identified as an extension of moist air into a drier region on a selected isentropic surface. A typical example from their studies is adapted in Fig. 1, which shows an MT from the southwest intersecting a DT from the northeast on the 315-K isentropic surface over North America in mid-September 1936. These isentropic charts were produced by drawing on the maps the elevation contours of a selected isentropic surface (e.g., 315 K) and the specific humidity, both interpolated from available upper-air observations. The coherent moisture-flow pattern in Fig. 1 is often associated with cloudiness and precipitation. Its elongated shape bears a strong resemblance to an inland-penetrating AR across central North America (e.g., Moore et al. 2012, 2015; Mahoney et al. 2016; Mo and Lin 2019). Note that the elevated core of a typical AR is located around 1 km above mean sea level (MSL) (Ralph et al. 2004). Although the mean elevation of the 315-K surface in Fig. 1 is about 3–4 km MSL, the core of the MT is below 1.5 km MSL.

Through the novel use of isentropic analysis, Rossby’s team recognized the significance of the MTs in atmospheric dynamics and operational weather forecasting. The discovery of this synoptic-scale feature immediately aroused extensive theoretical and practical interests across the communities of meteorology, hydrology, and aviation (e.g., Osmun 1937; Byers 1938; Wexler and Namias 1938; Namias 1938, 1939a; Denham and Knoll 1939; Rossby

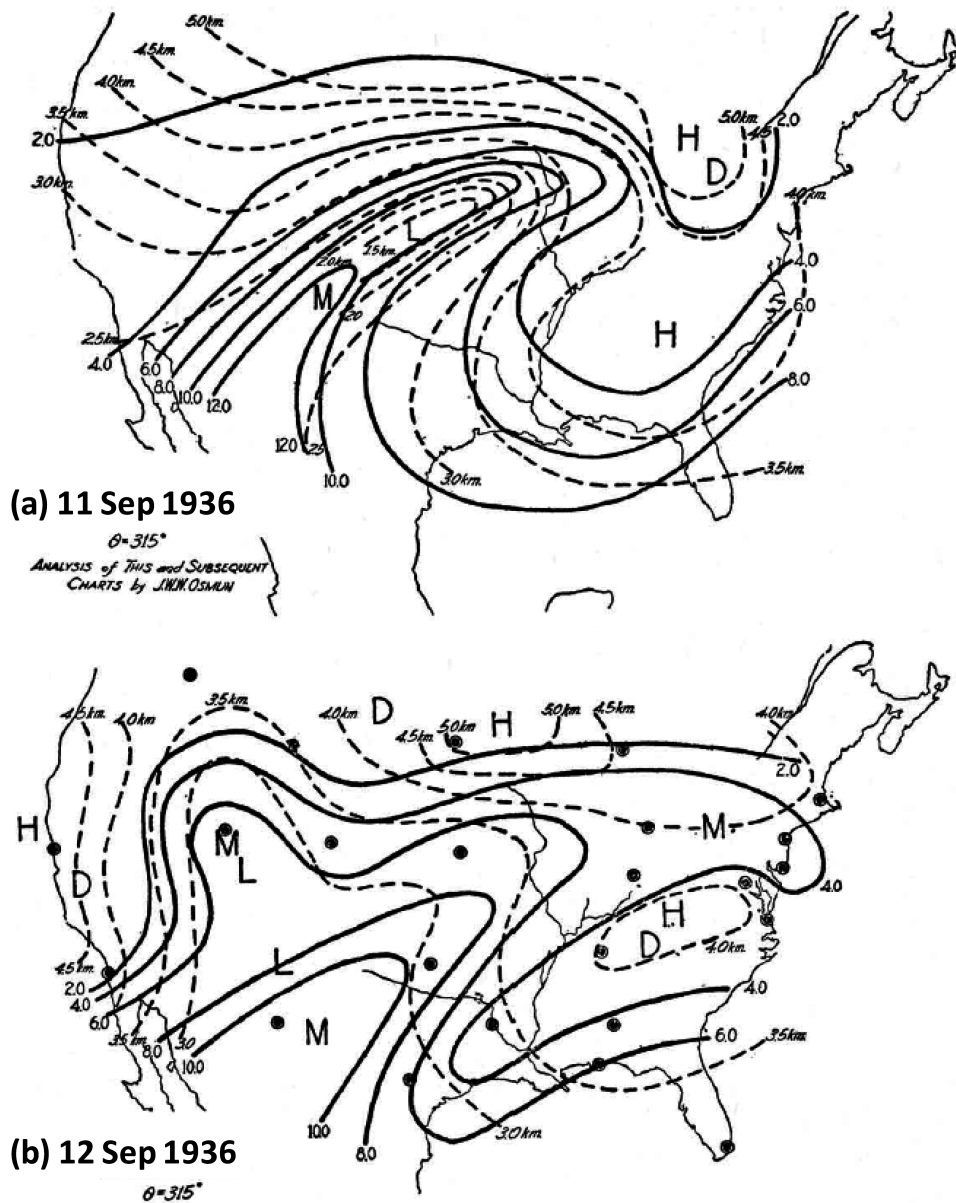


Fig. 1. The 315-K isentropic charts valid on (a) 11 and (b) 12 Sep 1936, adapted from Rossby et al. (1937b, Figs. 4 and 5; published 1937 by the American Meteorological Society). The solid lines are specific humidity contours ( $\text{g kg}^{-1}$ ; intervals:  $2 \text{ g kg}^{-1}$ ). The dashed lines are contours of height (above mean sea level) of the isentropic surface in km (intervals:  $0.5 \text{ km}$ ). The letters M and D stand for moist and dry (specific humidity). The letters H (for high) and L (for low) refer to the topography of the isentropic surface. The upper-air data used to produce these charts were observed at the 24 aerometeorological stations indicated by dots in (b).

et al. 1939; Weightman 1939, 1940; Bernard 1940; Haynes 1940; Petterssen 1940; Swenson 1940; Knarr 1941; Mitchell and Wexler 1941; Willett et al. 1941; Starr 1942; Showalter and Solot 1942; Means 1944; Showalter 1944). One successful application of the MT analysis was immediately found in the forecasting of summertime precipitation. Based on a case study in the summer of 1937, Namias (1938) pointed out that a weak MT may suffer lateral mixing with the dry air flanking it on both sides, which could act against thunderstorm formation and restrict the showers to its very central portion; on the other hand, strong MTs may remain comparatively unaltered by lateral mixing, and thereby provide ideal regions for continued thunderstorm activity (also see Rossby et al. 1938; Wexler and Namias 1938; Haynes 1940). For winter precipitation, Namias (1939a) showed a tongue of moist and warm air flowing northeastward over the eastern Gulf States during 6–8 December 1938; aloft, this MT was

displaced by a cold DT from the west, and the established conditional instability (Rossby and Weightman 1926) resulted in thundershowers in northern Florida.

Unfortunately, the isentropic analysis advocated by Rossby's team in the 1930s was supplanted by isobaric analysis for operational purposes after 1945, mainly because the isentropic charts were difficult to produce in the precomputer age (for some other reasons, see Bleck 1973). As a consequence, the enthusiasm for the isentropic MT analysis has also faded away (e.g., Brooks 1945; Jones and Roe 1953; Namias 1955; Semonin 1960; Fritz 1961; Leese 1962; Mills 1989; Clark et al. 2005; Cerveny et al. 2011; Jeong et al. 2014). On the other hand, MTs as a meteorological phenomenon have been mentioned by some researchers using the isobaric analysis or other techniques (e.g., Takahashi et al. 1954; Saito 1966; Chang 1971; Namias and Wagner 1971; Miller 1973; Carleton 1985; Wernli 1997; Lau et al. 1998; Waugh 2005; Du et al. 2020).

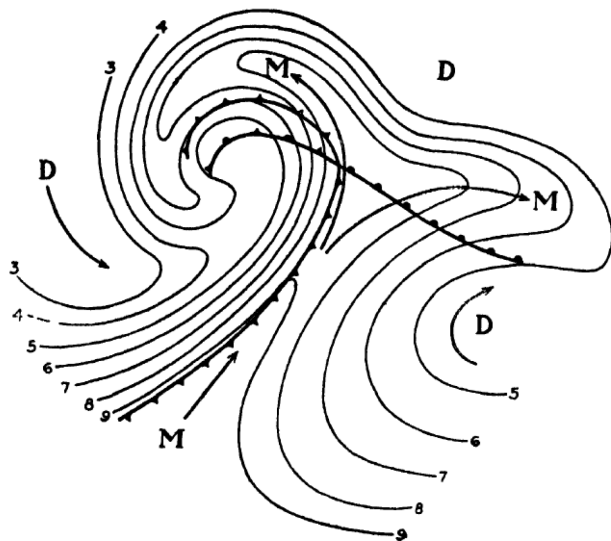
There are several important properties shared by the phenomena of MTs, WCBs, and ARs, as conceptually illustrated in Fig. 2. They are all identified as an elongated stream of moist air. They are often related to an extratropical cyclone and the associated fronts. Most importantly, they all have the potential to produce heavy and sometimes prolonged precipitation. Since the MT notion was introduced in 1937, it may be considered as a prequel to the modern theories of WCBs (since 1971) and ARs (since 1992). It is from this historical perspective that I would like to reexamine the classic MT model of the Rossby school and establish a connection of this isentropic tradition with the modern theories of WCBs and ARs. There have been recent articles that attempt to compare and distinguish among ARs, WCBs, and TMEs (e.g., Dettinger et al. 2015; Browning 2018; Ralph et al. 2018, 2020). However, the MT model developed in the 1930s has not received enough attention. Wernli (1997) pointed out that the analysis of the conveyor-belt model (Browning 1971; Harrold 1973; Carlson 1980) is based on the traditional isentropic analysis developed in the 1930s (also see Wernli and Davies 1997). The term MT was used by Browning and Hill (1985) in their isentropic analysis of the conveyor belts associated with a polar front, and in a later study Browning (1990) recognized that the conveyor belt model can be related to the isentropic MT/DT model presented in Namias (1939b), which is almost the same as Fig. 2a. This model was also cited by Ralph et al. (2004) and Fu et al. (2021) in their AR studies. Zhu and Newell (1994) noticed the similarity between the AR structure and a narrow tongue of moisture described by Starr (1942). Nevertheless, the detailed features of this isentropic MT model were not sufficiently discussed in these studies.

The first objective of this article is to present a comprehensive review of the literature related to the identification, conceptual model, and applications of MTs in the "isentropic era." As expected, the isentropic MT model is indeed related to the current models of WCBs and ARs. However, stark differences among these three phenomena do exist based in part on how they are defined and diagnosed (e.g., isentropic, isobaric, or vertically integrated). One clear difference is that an MT can be quite elevated and contribute to more synoptic-scale precipitation along the WCB, whereas ARs are almost always lower tropospheric phenomena with water vapor transport driven by the LLJ. My second objective is to demonstrate in two case studies how an MT can be similar to an AR and how they can be quite different under certain circumstances. Some limitations of the isentropic MT analysis will be noted and discussed in these case studies.

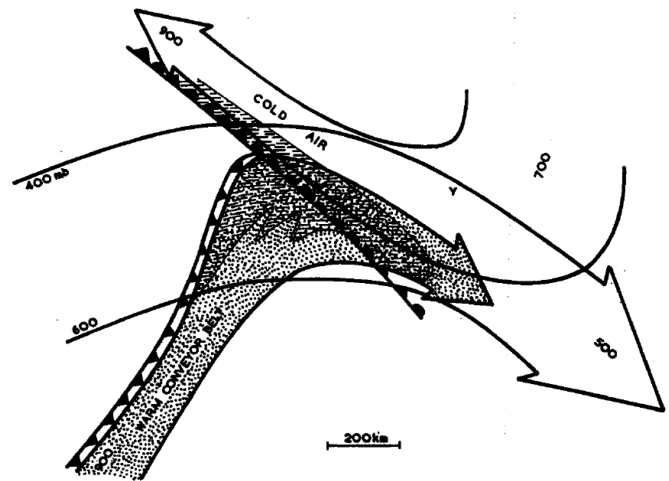
### **Isentropic charts and the moist/dry tongues**

Isentropic analysis is a meteorological technique for examining air motion during an adiabatic process above the planetary boundary layer. A common practice is to plot some variables on a surface of constant potential temperature (isentropic surface). This approach was first suggested by Sir Napier Shaw (Shaw 1929). A practical procedure for drawing isentropic weather maps was later proposed in Shaw (1930, 259–263). The potential of this innovation was quickly recognized by Rossby (1932), who proposed a simple graphical method for air mass analysis by means of two conservative quantities: potential temperature and specific humidity.

(a) Moist tongue model



(b) Warm conveyor belt model



(c) Atmospheric river model

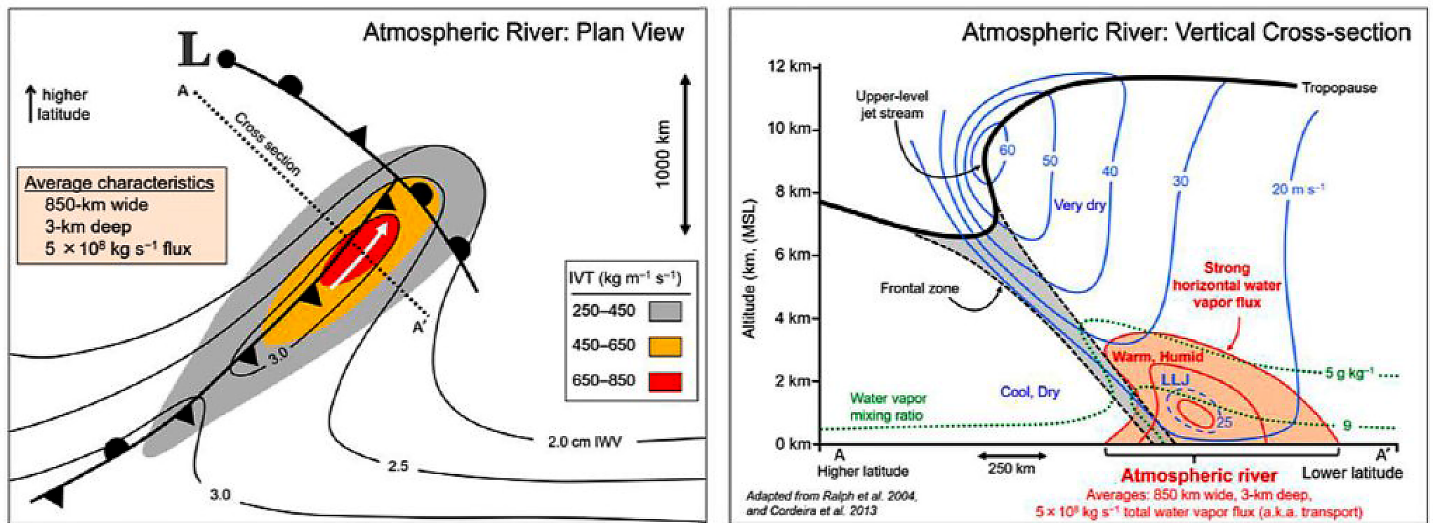


Fig. 2. Conceptual models of the MT, WCB, and AR. (a) Schematic flow pattern around an occluded cyclone as shown by surface fronts and moisture lines in an isentropic surface, reproduced from Namias (1940, Fig. 182, p. 364; ©McGraw Hill; used with permission); the solid lines represent constant specific humidity ( $\text{g kg}^{-1}$ ), and the arrows indicate the instantaneous flow of dry (D) and moist (M) currents. (b) Conveyor belt model adapted from Browning (1971, plan view of Fig. 3, p. 321; ©John Wiley and Sons; used with permission); stippled shading represents the warm conveyor belt and hatched shading depicts the extent of precipitation. (c) Schematic summary of the structure and strength of an atmospheric river, adapted from Ralph et al. (2017b, Fig. 16, p. 2594; ©American Meteorological Society; used with permission); the left panel is a plan view, and the right panel is a vertical cross-section view.

When the aerological network of the United States reached a state to permit a practical test of the value of isentropic analysis, Rossby et al. (1937a,b) took a key step by plotting specific humidity data on some selected isentropic surfaces. They argued that, since both potential temperature and specific humidity are invariant with adiabatic processes, many features of air motion in the free atmosphere could be visualized by plotting the specific humidity on isentropic surfaces. The procedure involved 1) drawing an equivalent potential temperature diagram for each individual airplane sounding, where the values of weather elements at a fixed potential temperature are determined by interpolation, and 2) plotting these values on a regional map for air motion analysis (Osmun 1937; Rossby et al. 1937b).

Based on the upper-air observations from 24 aerometeorological stations across the United States, Rossby et al. (1937a,b) produced six isentropic charts for two synoptic situations during

11–15 September 1936. Their first two charts are shown in Fig. 1. Note that the exact valid hour for each map was not mentioned, because the data used to produce the map were observed over a period of several hours. Detailed analysis of these isentropic charts led to the following conclusions: 1) isentropic flow patterns are simpler than corresponding frontal systems on surface maps, and they change only slowly from day to day thanks to their material nature; 2) isentropic surfaces act like material sheets over a period of a few days, except for some small areas along active fronts or convection centers where the release of latent heat due to condensation cannot be ignored; 3) both MTs and DTs are evident on the isentropic surfaces; and 4) MTs or DTs advance less rapidly than expected from the observed wind distribution, indicating intense lateral mixing in the atmosphere (the assumption of adiabatic motion implies that each element of air remains in its proper isentropic layer).

In particular, these two studies directed the attention of meteorologists to the large-scale MTs and their application potential in short- and long-range weather prediction. As shown in Fig. 1a, the situation on 11 September 1936 is characterized by the northeastward advance of an MT from the southwestern United States on the 315-K isentropic surface. This tongue reaches the Atlantic Coast on the next day (Fig. 1b) after having intersected a DT from the north. It was noticed that the lines of constant specific humidity and height contour lines are nearly parallel in most areas, and regions of vertical motion and significant precipitation may be determined from the intersection of these two sets of lines on the isentropic charts (Rossby et al. 1937b). This statement only makes sense for the large-scale geostrophically balanced flow. The diabatic processes associated with strong convection and precipitation in the vicinity of a cold front may disturb the conservative nature of the isentropic charts, because the addition of moisture through convection or loss by precipitation cannot be avoided in some areas. As pointed out in Rossby et al. (1937a), a significant portion of the high moisture content with the MT in Fig. 1 is likely caused by the intense vertical mixing attending the passage of tropical air across the Mexican mountains.

### **Isentropic cross sections for MT analysis**

Rossby et al. (1938) pointed out that the term “isentropic analysis” should apply not only to the study of upper-air charts for prescribed isentropic surfaces, but also to the interpretation of atmospheric cross sections, without which the analysis would be incomplete. They further argued that, in order to take full advantage of the cross sections, it is necessary to make use of the two most conservative properties, potential temperature ( $\theta$ ) and specific humidity ( $q$ ). A schematic picture of such a  $\theta$ - $q$  cross section from their study is reproduced in Fig. 3. In these diagrams, the solid and dashed lines represent specific humidity and potential temperature, respectively. Their usefulness for convection diagnosis was assessed by Jerome Namias (Rossby et al. 1938, 35–36):

The fact that convection due to heating from below lowers the isentropic surfaces but raises the specific humidity at any fixed level makes the isentropic cross sections especially helpful in locating regions of significant convective activity. In these regions the moisture lines of the cross section bulge upward while the lines of constant potential temperature dip downward...

Figures 4 and 5 provide a real example adapted from Rossby et al. (1938). They were produced from the upper-air data collected from pilot balloon ascensions for about 110 stations in North America and some daily airplane meteorograph flights between Canada and the United States during 22–23 May 1936. These observations were not synchronous but most of them were taken in the morning hours between 0400 and 0800 EST (0800 and 1200 UTC). The two isentropic charts show an impressive MT (No. 9) extending northward from the Gulf of Mexico to the Great Lakes region. Its shape and scale are suggestive of an inland-penetrating AR (e.g.,

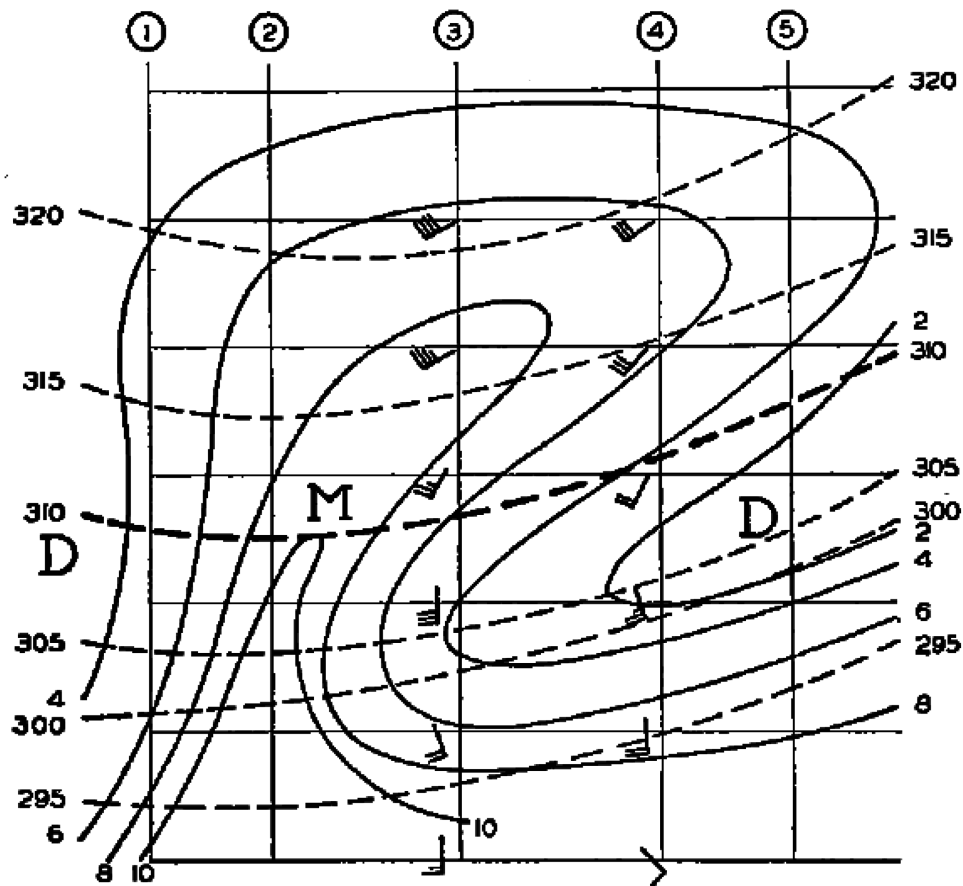


Fig. 3. Schematic cross section through a convective area, reproduced from Rossby et al. (1938, Fig. 4 in section B, p. 27; used with the permission of Woods Hole Oceanographic Institution). The solid lines are specific humidity contours ( $\text{g kg}^{-1}$ ; intervals:  $2 \text{ g kg}^{-1}$ ). The dashed lines are potential temperature contours (K; intervals:  $5 \text{ K}$ ). The letters M and D stand for moist and dry. Wind speed and direction are indicated by the conventional wind barbs.

Mo and Lin 2019). Widespread thunderstorms were reported along this moist flow. The two isentropic cross sections show that the core of this MT was located near Earth's surface. In Fig. 5a, the two elevated maximum centers of specific humidity between 310 and 315 K (over Omaha and San Antonio, respectively) were likely caused by strong convection along the MT.

Rossby et al. (1938) noticed that precipitation is often caused by the MT running up the steep isentropic slope. Most of continuous (stratiform) precipitation occurs on the northern side of the MTs. This is usually due to the motion of moist air up the slope of a warm front. The distribution of thunderstorms, however, may follow the flow patterns much more closely. Especially in the warm season, the mere presence of an MT, irrespective of whether or not it is flowing upslope, is often sufficient to give thunderstorms.

### Diabatic effects

The isentropic analysis of the Rossby school is built on the basic assumption of adiabatic motion, which implies that each element of air remains in its proper isentropic layer in the free atmosphere. However, diabatic influences cannot always be neglected. Rossby et al. (1938) recognized three fundamental diabatic processes that may need to be addressed carefully in isentropic analysis: 1) radiation, 2) convection, and 3) condensation and evaporation. Their discussions related to radiation and the diabatic effects of precipitation processes are omitted here for clarity. Convection needs more attention; it is an important diabatic process involving strong vertical (cross-isentrope) mass transport.

The role of convection is to transfer heat and moisture upward through the atmosphere. The moisture pumped aloft by convection may be carried far from its source by currents in

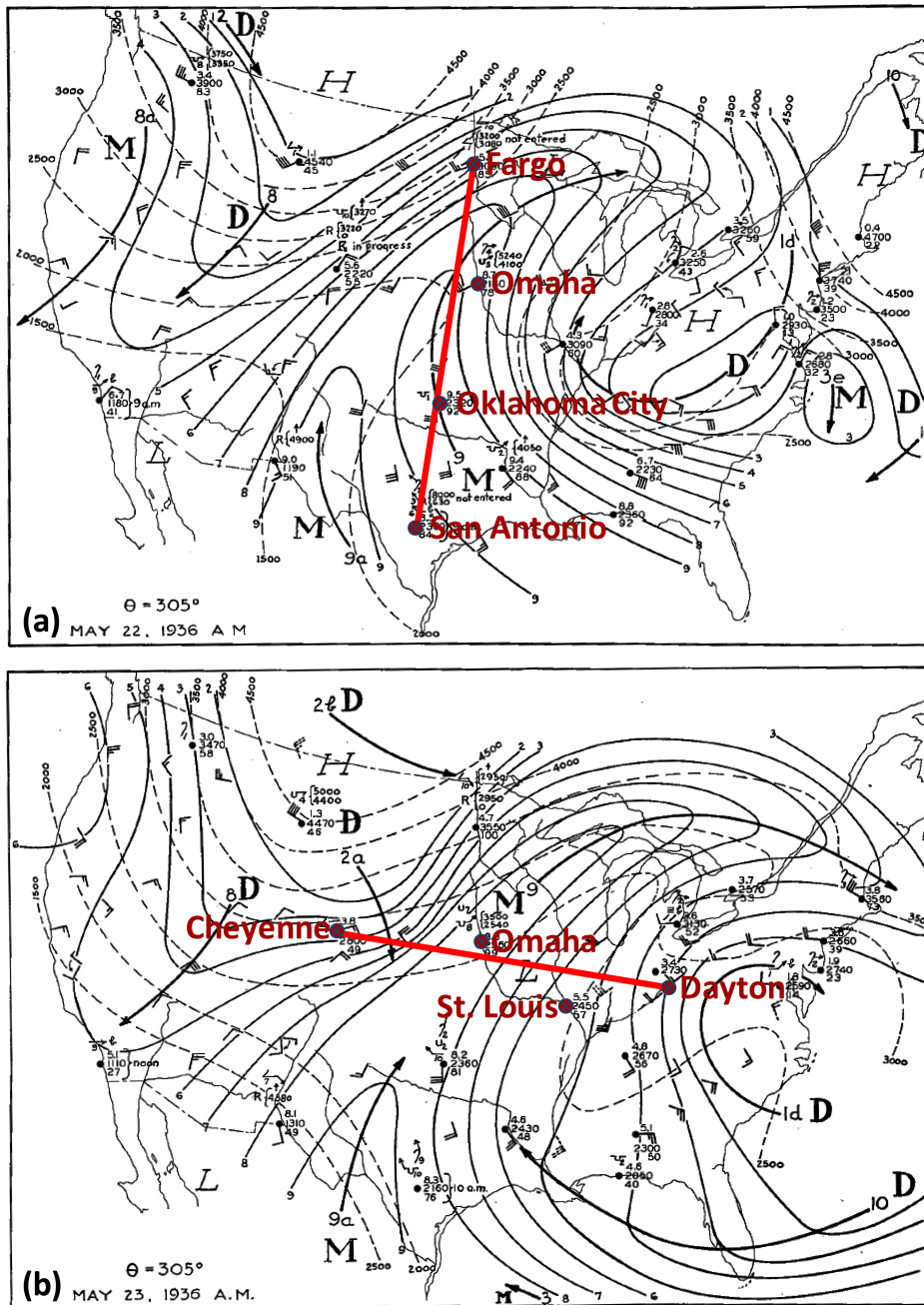
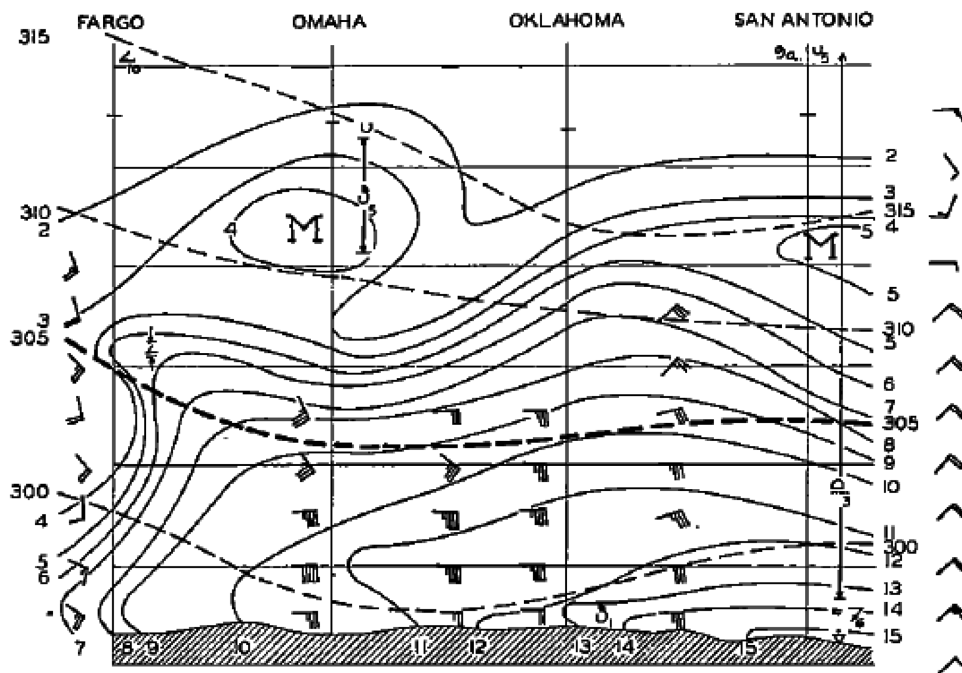


Fig. 4. The 305-K isentropic charts valid the mornings of 22 and 23 May 1936, adapted from Rossby et al. (1938, Plates XIV and XV of section C; used with the permission of Woods Hole Oceanographic Institution). The solid lines are specific humidity contours with intervals of  $1 \text{ g kg}^{-1}$ . The dashed lines are height contours with intervals of 500 m. The moist (M) and dry (D) tongues are numbered and indicated by line arrows. The two red lines and eight reference stations are added to indicate the cross-section lines in Fig. 5.

the free atmosphere, so that the moisture lines of the cross sections in the region of violent convection frequently display a pattern similar to the anvil structure of the thunderstorm clouds (Rossby et al. 1938). The importance of convection in maintaining the MTs was further emphasized by Rossby et al. (1938, 36–37):

If it were not for the replenishment of moisture by convective transport upward, the moist tongues of the isentropic charts would soon be robbed of their vapor through lateral mixing with the dry air flanking them on both sides. In summer time thunderstorms may truly be considered as the life blood of the moist currents.

(a) 22 May 1936, from Fargo, ND to San Antonio, TX



(b) 23 May 1936, from Cheyenne, WY, to Dayton, OH

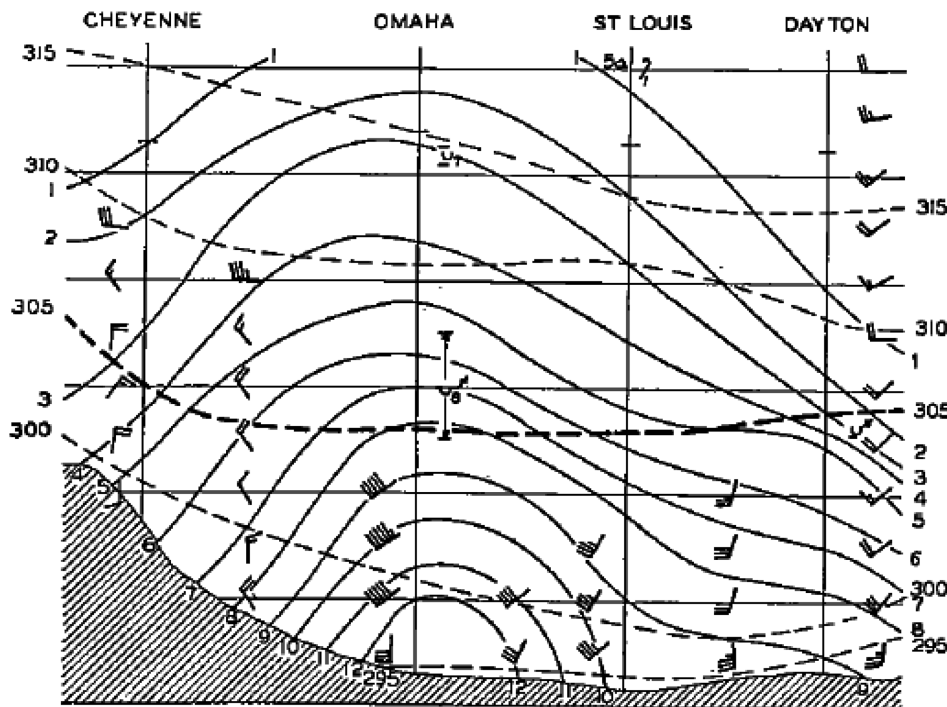


Fig. 5. (a) A north-south vertical cross section (from Fargo, North Dakota, to San Antonio, Texas) valid on 22 May 1936, adapted from Rossby et al. (1938, Plate V of section C). (b) A west-east vertical cross section (from Cheyenne, Wyoming, to Dayton, Ohio) valid on 23 May 1936, adapted from Rossby et al. (1938, Plate VI of section C). The solid lines are specific humidity contours (intervals:  $1 \text{ g kg}^{-1}$ ). The dashed lines are potential temperature contours (intervals:  $5 \text{ K}$ ). The letters M and D stand for moist and dry. Winds are indicated by the conventional wind barbs. These figures are used with the permission of Woods Hole Oceanographic Institution.

**The interactions of MTs with anticyclonic and cyclonic eddies**

The interactions among MTs, DTs, cyclones, and anticyclones formed an important part of the isentropic analysis in the 1930s. It was suggested in Rossby et al. (1938, p. 29) that the

formation of large-scale anticyclones and cyclones could be explained based on the principle of conservation of absolute circulation:

Thus the total absolute circulation of any isentropic fluid chain consists of a circulation relative to the earth plus the circulation of the earth itself about this chain. If there are no frictional forces and if the motion is strictly adiabatic this sum must remain constant. Thus, if an originally stationary isentropic fluid chain is displaced from equatorial to polar regions it must develop an anticyclonic sense of circulation relative to an observer on the earth in order to counterbalance the increased circulation of the earth itself around the chain as it moves northward. Similarly, a southward moving system tends to develop a cyclonic circulation.

The above statement is just the Bjerknes circulation theorem (Bjerknes 1898, 1902) applied on an isentropic surface. It was the basis for the Rossby wave theory to be developed in the years to come (Rossby 1939, 1940, 1941; Hoskins et al. 1985). For its application to the MT/DT analysis, Namias (1940, p. 147) used a schematic flow pattern (see Fig. 2a) to summarize the main features of a typical MT and its interactions with other components surrounding an occluded cyclone:

The moist current, having come up from the south, tends to acquire anticyclonic curvature indicated by the directional flow arrow to the upper right... Where the polar air intrudes into the system from the north it develops cyclonic vorticity... Thus a branch of the moist flow is diverted from the mother current into the cyclonic flow...

This description bears a close resemblance to the intersection of the warm and cold flows in the conveyor belt model developed a few decades later (e.g., Browning 1971, 1986; Carlson 1980; Stewart and Macpherson 1989). Martínez-Alvarado et al. (2014) found that the WCB of an extratropical cyclone generally splits into two branches; whether it turns cyclonically or anticyclonically depends on the altitude at which air exits the WCB. In Fig. 2a, the MT ahead of the cold front is what we call an AR today.

### **Comparisons of MTs with ARs: Two case studies**

Despite the apparent similarity between the MT model and the AR (or WCB) model (Fig. 2), there are important differences in pattern recognition, classification, and practical applications. MTs can be visually recognized as some elongated areas of maximum specific humidity on selected isentropic charts. Their shape and intensity may vary significantly depending on the selected isentropic surface, and it is not easy to define lateral boundaries for an MT. The ARs, on the other hand, are often objectively identified from the distributions of vertically integrated water vapor (IWV) or integrated vapor transport (IVT) with some specific criteria. A popular method known as  $IWV_{20}$  defines an AR as an area with IWV greater than  $20 \text{ kg m}^{-2}$ , narrower than 1,000 km, and longer than about 2,000 km (Ralph et al. 2004). This method has since been replaced by the IVT methods that use both restrictive thresholds (e.g., the  $IVT_{250}$  in Rutz et al. 2014) and flexible thresholds [e.g., the location and season dependent 85th percentile in Guan and Waliser (2019)]; see Shields et al. (2018) for an in-depth comparison of various AR identification techniques.

In this section, two case studies are performed to show how an MT can sometimes overlap with or distinguish from an AR. The first case is the synoptic situation during 22–23 May 1936 (Figs. 4 and 5). The second case is the situation during 11–12 September 1936 (Fig. 1).

**Data description.** Two datasets are used in these two case studies. The first is version 3 of the NOAA–CIRES–DOE Twentieth Century Reanalysis (20CRv3) produced by an assimilation

system that assimilates only surface pressure reports with observed monthly sea surface temperature and sea ice distributions to generate a global atmospheric dataset (Compo et al. 2011; Slivinski et al. 2019). This reanalysis provides 8-times daily data from 1836 to 2015 on a  $1^\circ$  latitude  $\times$   $1^\circ$  longitude grid. It can reliably produce atmospheric estimates on scales ranging from weather events to long-term climatic trends (Slivinski et al. 2021). The isentropic analysis and vertical integration scheme can be easily performed using this three-dimensional (3D) dataset. There are some known issues with 20CRv3, including a systematic bias in tropical precipitation (Slivinski et al. 2019) and substantial biases in temperature and wind above 300 hPa (Slivinski et al. 2021). Note that the isentropic analysis in the 1930s relied on the upper-air data from the newly established aerological network in North America. These upper-air data, however, were not included for assimilation to produce 20CRv3. This limitation could have an impact on the MT and AR analyses in the case studies. In addition, the coarse resolution ( $1^\circ \times 1^\circ$ ) would render 20CRv3 inappropriate for analyzing convective precipitation.

The second dataset includes the daily precipitation amount in North America. It is extracted from the Global Historical Climate Network-Daily (GHCN-Daily) summaries provided by the National Centers for Environmental Information ([www.ncdc.noaa.gov/cdo-web/](http://www.ncdc.noaa.gov/cdo-web/)). This quality-controlled dataset includes daily observations around the world. It is developed to meet the needs of climate analysis and monitoring studies at a submonthly time resolution.

**Case 1: MTs and ARs during 22–23 May 1936.** The 305-K isentropic charts for the mornings of 22 and 23 May 1936 in Fig. 4 are adapted from Rossby et al. (1938). Their reanalysis counterparts (20CRv3 valid at 1200 UTC) are shown in Figs. 6a and 6b. A comparison between them indicates that the geographical positions of the MTs are consistent. However, the ones in Fig. 4 are drier than those in Fig. 6. For instance, the maximum specific humidity across the U.S.–Mexico border (western Texas) is higher than  $11 \text{ g kg}^{-1}$  in Fig. 6a, but lower than  $10 \text{ g kg}^{-1}$  in Fig. 4a. A possible explanation for this difference is that the upper-air data are not assimilated into 20CRv3, leading to incorrect estimates of moisture distribution. This could be an inherent problem associated with this reanalysis, which takes only surface pressure observations into account (Slivinski et al. 2021).

Also shown in Fig. 6 are the distributions of mean sea level pressure (MSLP), IWV, and IVT valid at 1200 UTC 22–23 May 1936. An inland-penetrating AR across the central United States and eastern Canada can be identified using either the  $\text{IWV}_{20}$  or  $\text{IVT}_{250}$  rules. It was driven northeastward by a weakening cyclone-anticyclone couplet. This AR is well consistent with the isentropic MT in Figs. 6a and 6b. There was also a weak Pacific AR making landfall on the west coast of Canada on Figs. 6d and 6f. The corresponding MT is barely noticeable, given that elevations of the 305-K isentropic surface in that area are generally higher than 3,500 m MSL (Fig. 6b).

Figure 7 shows two vertical cross sections from 20CRv3, on which potential temperature, specific humidity, and wind are drawn in the same fashion as in Fig. 5. An extra element, the water vapor flux, is also included to highlight the fact that AR is a corridor of strong horizontal water vapor transport. The north–south cross section in Fig. 7a indicates that the AR core is located in the lower atmosphere around the 900-hPa level. At the southern end, the Mexican Plateau acts as a barrier to block moist flow from the tropical Pacific, and as a wall to guide moisture from the Gulf of Mexico into the United States. Toward the northern end, moisture lines bulged upward as the AR flowed onto a warm front marked by the strong horizontal gradient of potential temperature. The west–east cross section in Fig. 7b shows that the AR was ahead of a cold front. The prefrontal convection forced the moisture lines to bulge upward over the AR.

The corresponding 24-h precipitation amounts from the 20CRv3 and the GHCN-Daily observations are plotted in Fig. 8. Although the reanalysis has an AR-induced maximum center of moderate (25–50 mm) to heavy (>50 mm) precipitation in the midwestern United States, it seriously underestimates precipitation intensity along the AR axis. In particular,

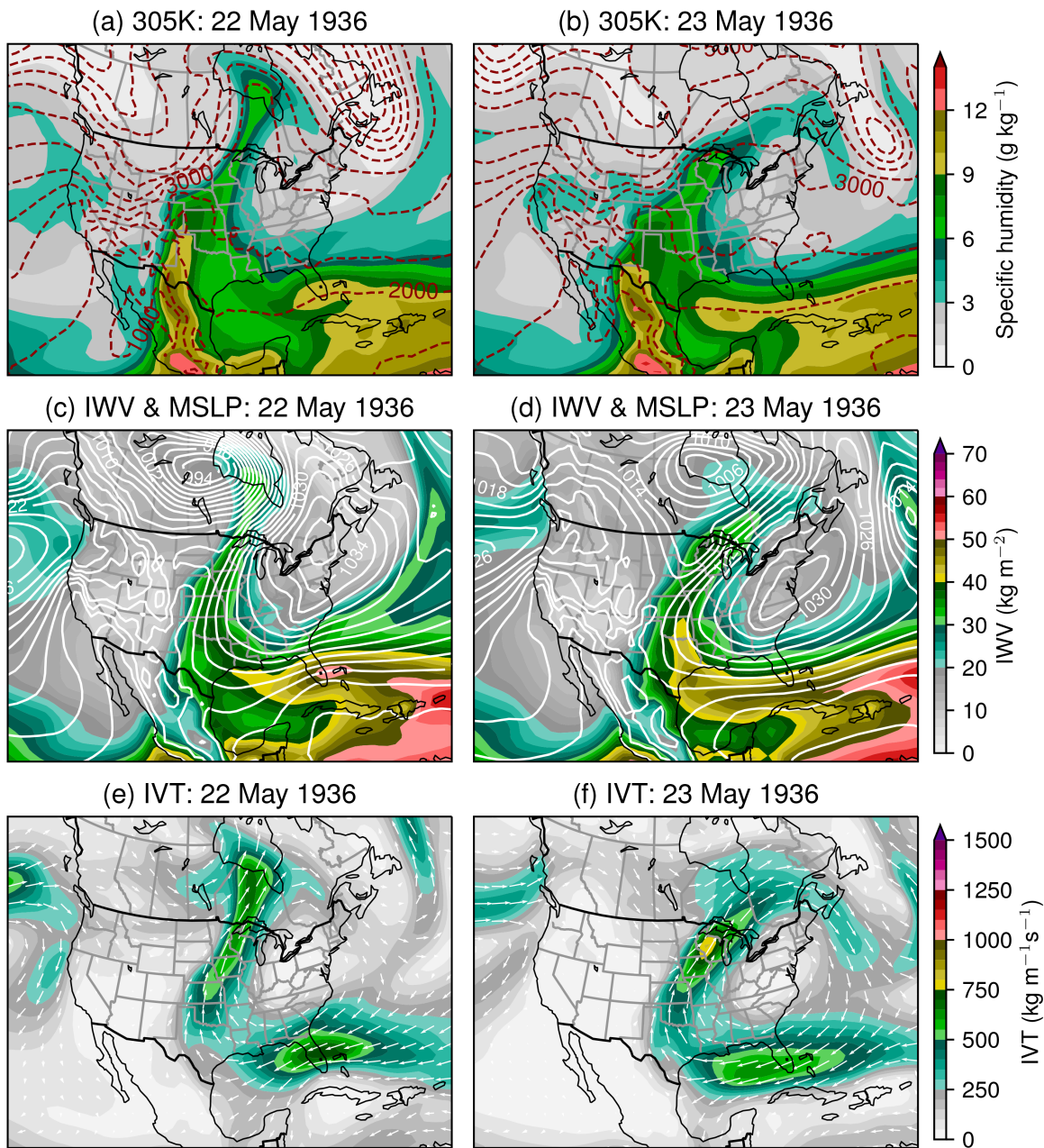


Fig. 6. MT and AR analysis based on the 20CRv3 data valid at 1200 UTC 22 and 23 May 1936. (a),(b) The 305-K isentropic charts, where the color-filled contours ( $\text{g kg}^{-1}$ ) show the specific humidity distribution and the red dashed lines are contours of height (above mean sea level) of the isentropic surface (m; intervals: 500 m). (c),(d) The IWV (color filled;  $\text{kg m}^{-2}$ ) and MSLP (white solid lines; intervals: 2 hPa). (e),(f) The vertically integrated water vapor flux (white vector) and its magnitude known as IVT (color filled;  $\text{kg m}^{-1} \text{s}^{-1}$ ). The range of vertical integration for IVT is from Earth's surface to the 100-hPa level.

much higher amounts were observed over coastal Texas, with the highest value of 273.1 mm at Schulenburg (29.68°N, 96.86°W). Overall, there are 37 stations reporting a daily amount greater than 50 mm, with six of them with an amount exceeding 100 mm. On the other hand, the differences between reanalysis and observations are acceptable over Florida and the west coast of Canada.

**Case 2: MTs and ARs during 11–12 September 1936.** The isentropic MT and AR analyses from 20CRv3 for the situations on 11–12 September 1936 are shown in Figs. 9 and 10. The reanalysis MTs in Figs. 9a and 9b are geographically consistent with, but drier than, their counterparts in Fig. 1; the drier conditions of 20CRv3 in this case are in contrast to the moister conditions in the previous case.

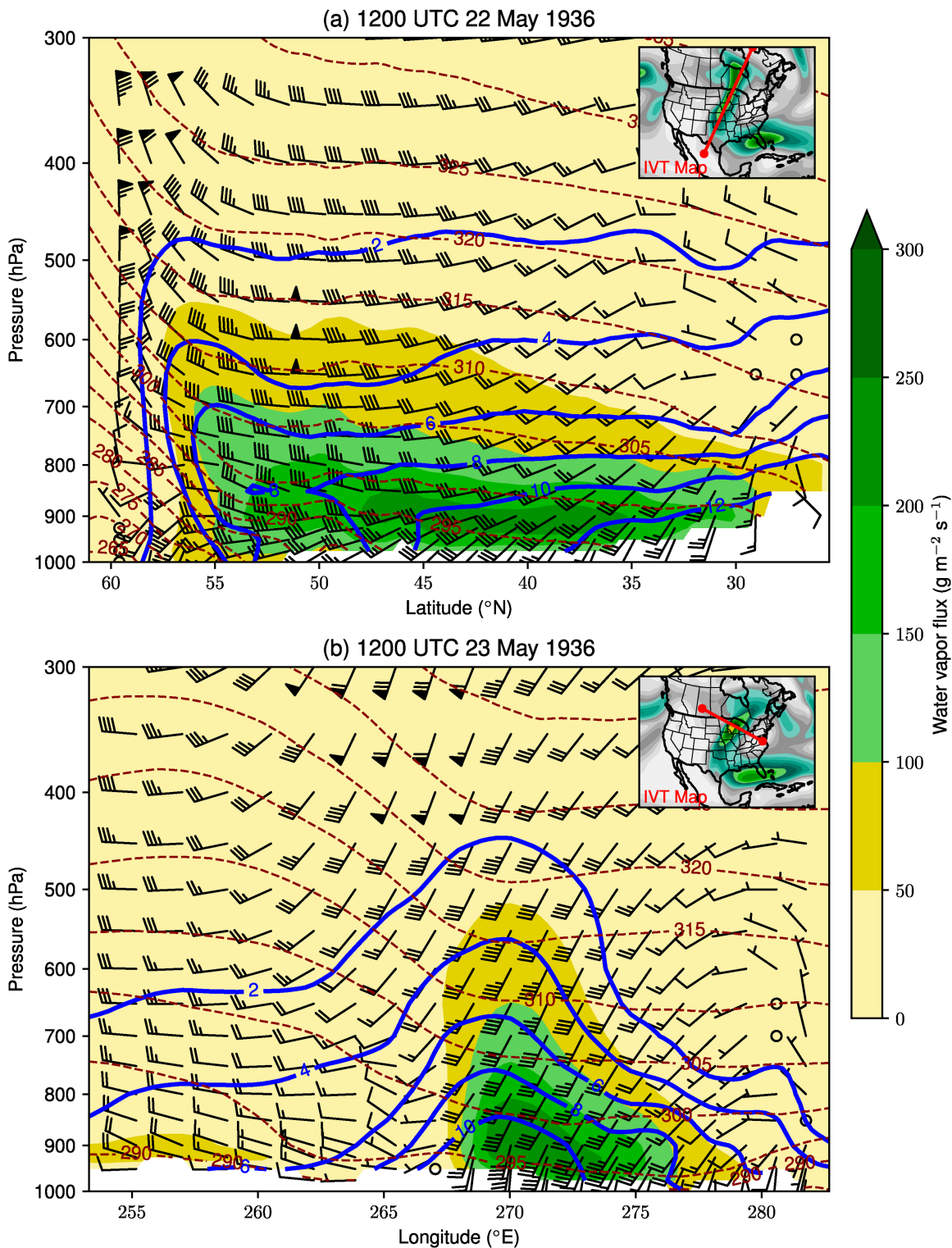
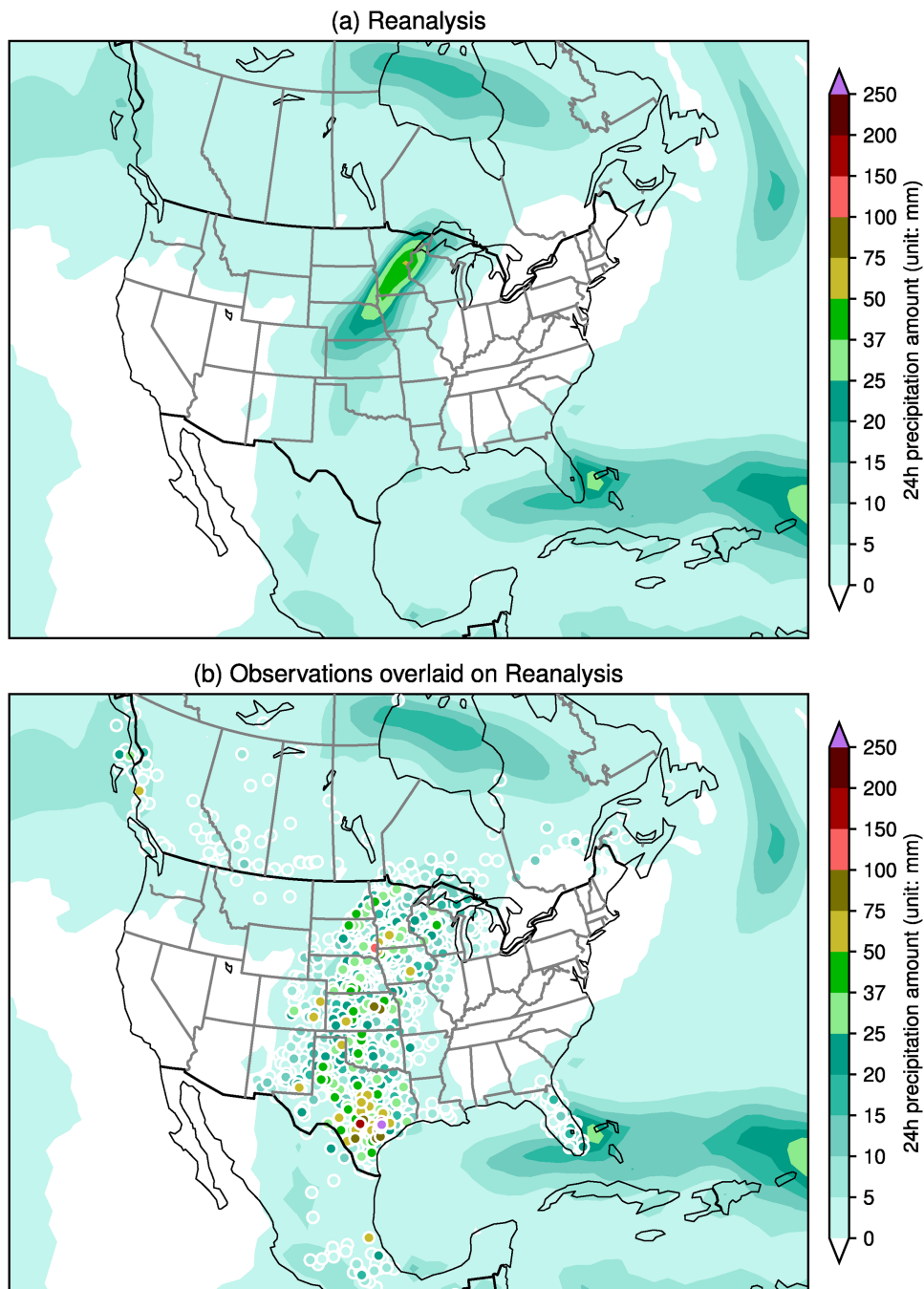


Fig. 7. (a) A north–south vertical cross section (from Quaqtaq, Quebec, Canada, to Torreón, Mexico) valid at 1200 UTC 22 May 1936. (b) A west–east vertical cross section (from Calgary, Alberta, Canada, to Richmond, Virginia) valid at 1200 UTC 23 May 1936. The blue solid lines are specific humidity contours (intervals:  $2 \text{ g kg}^{-1}$ ). The red dashed lines are potential temperature contours (intervals:  $5 \text{ K}$ ). The magnitude of water vapor flux is represented by color-filled contours. Winds are indicated by the conventional wind barbs. The cross-section line is indicated by a red line in the embedded box with IVT distribution.

The distributions of IVT in Figs. 9e and 9f (and IWV in Figs. 9c and 9d) suggest a weak to moderate AR over eastern North America. As compared to the corresponding MTs in Figs. 9a and 9b, the AR axis is located further to the east in the subtropical area, and the presence of



**Fig. 8.** (a) Accumulated precipitation amount (mm) for a 24-h period ending at 1200 UTC 23 May 1936 based on the 20CRv3 data. (b) The color-filled value is the same as in (a), while the observed daily precipitation amount is plotted to a colored dot; the observed amounts are plotted in ascending order to make sure that a heavier amount is overlaid on a lighter amount.

AR is more noticeable over eastern and Atlantic Canada, where the specific humidity values are low on the 315-K isentropic surface with elevations higher than 5,000 m. The isentropic analyses on the 305-K surface are shown in Figs. 10a and 10b. The MT locations on this lower level are more consistent with the AR positions in Figs. 9e and 9f.

The reanalysis in Fig. 10c shows generally light daily precipitation (less than 25 mm) along the MT/AR corridor, except for some moderate (25–50 mm) rains off the east coast of Mexico where a tropical cyclone can be seen in the MSLP maps (Figs. 9c,d). There is a local maximum of 20–25 mm in the southern Great Lake region. The observed daily precipitation amounts are much higher (Fig. 10d). The highest amount of 135.6 mm was observed at La Unión (17.98°N, 101.88°W) in southern Mexico. It is followed by an amount of 99.8 mm at

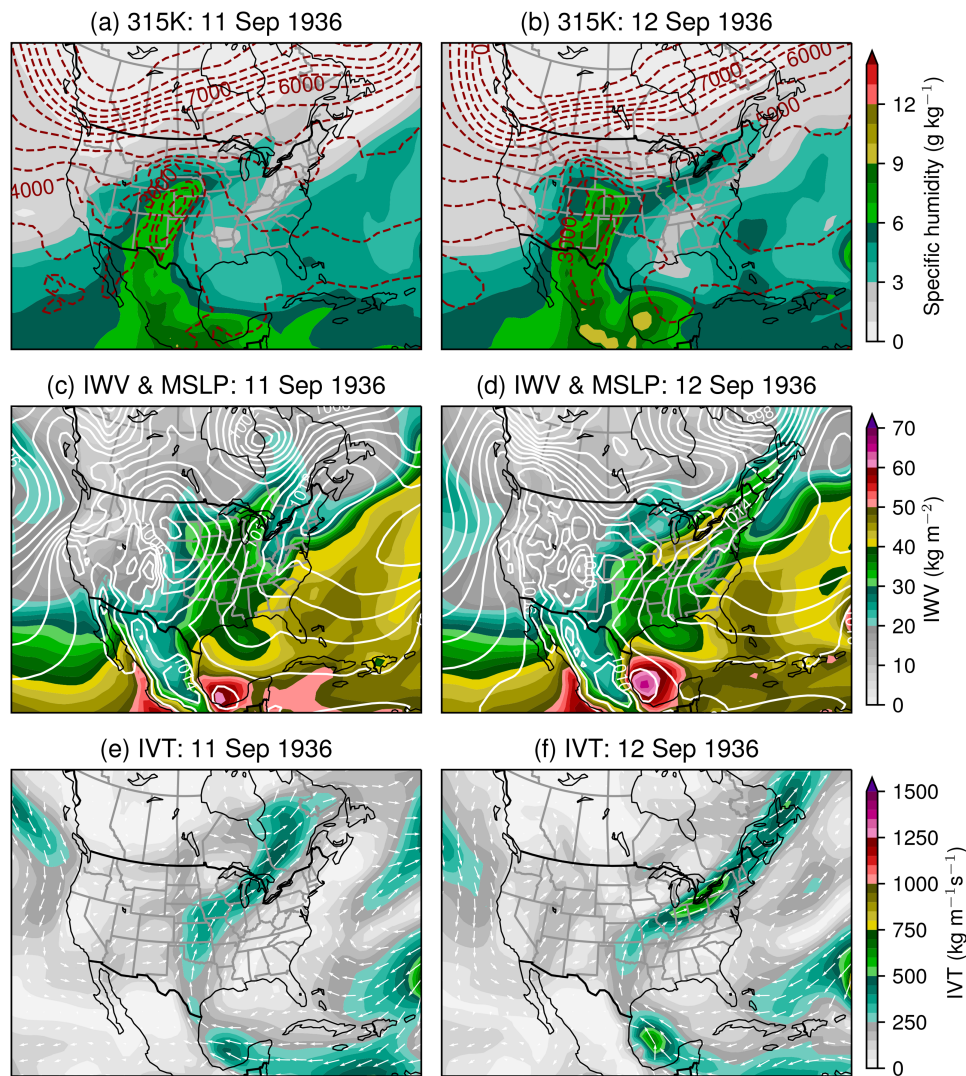
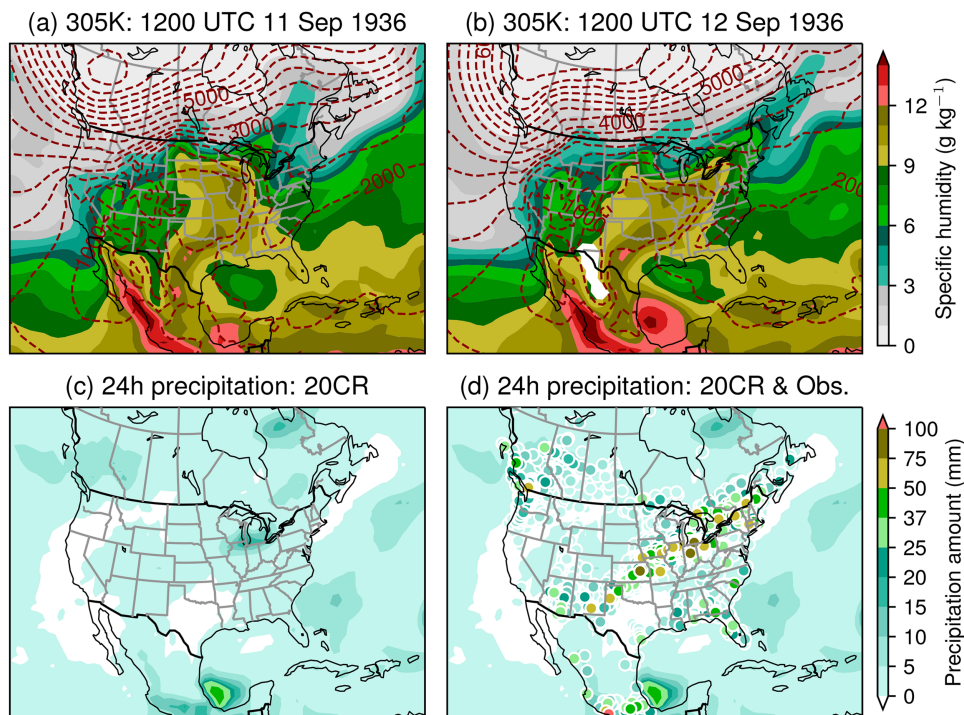


Fig. 9. MT and AR analysis based on the 20CRv3 data valid at 1200 UTC 11 and 12 Sep 1936. (a),(b) The 315-K isentropic charts, where the color-filled contours ( $\text{g kg}^{-1}$ ) show the specific humidity distribution and the red dashed lines are contours of height (above mean sea level) of the isentropic surface (m; intervals: 500 m). (c),(d) The IWV (color filled;  $\text{kg m}^{-2}$ ) and MSLP (white solid lines; intervals: 2 hPa). (e),(f) The vertically integrated water vapor flux (white vector) and its magnitude IVT (color filled;  $\text{kg m}^{-1} \text{s}^{-1}$ ).

Kokomo, Indiana ( $40.46^{\circ}\text{N}$ ,  $86.18^{\circ}\text{W}$ ). The third highest amount is 93.7 mm at Council Grove, Kansas ( $38.67^{\circ}\text{N}$ ,  $96.50^{\circ}\text{W}$ ), and there are 31 stations with observed daily amounts greater than 50 mm on the map.

## Conclusions

Carl-Gustaf Arvid Rossby was one of the most influential atmospheric and oceanic scientists in the twentieth century (Byers 1960). One of his scientific undertakings in the 1930s was the investigation of large-scale lateral mixing in the atmosphere. Following an earlier suggestion of Sir Napier Shaw, Rossby et al. (1937a,b) reasoned that lateral mixing would occur on isentropic surfaces, and these isentropic charts could be taken as a working tool for synoptic weather analysis. Using water vapor as a conservative tracer, their first application of isentropic analysis not only provided evidence of large-scale lateral mixing in the atmosphere, but also identified the moist tongues as an important flow pattern which can be used for tracing the sources of atmospheric moisture. They also suggested the use of isentropic cross sections to provide further insight into the vertical structure and dynamic stability of MTs (Rossby et al.



**Fig. 10.** (a),(b) The 305-K isentropic charts valid at 1200 UTC 11 and 12 Sep 1936 (compared to the 315-K charts in Figs. 9a,b). (c) Accumulated precipitation amount (mm) for a 24-h period ending at 1200 UTC 12 Sep 1936 based on the 20CRv3 data. (d) The color-filled value is as in (c), while the observed daily precipitation amount is plotted to a colored dot (see Fig. 8).

1937b, 1938). The present article established a historical narrative that would acknowledge the MT model developed in the 1930s as an antecedent to the contemporary concepts of WCB and AR. As shown in Fig. 2, these three phenomena are interrelated with a common feature of strong low-level moisture transport. Under certain circumstances, therefore, they are all but different manifestations of the same thing.

Jerome Namias was one of Rossby's most prominent collaborators in advocating for isentropic analysis. He was also part of a team devoted to developing reliable methods for short- and long-range weather forecasts (Wexler and Namias 1938; Namias 1938, 1939a,b, 1940; Willett et al. 1941). Their studies confirmed that an MT entering the United States from the Gulf of Mexico is an important factor to be considered in weather forecasting, and areas of heavy precipitation are often located in the zone between MTs and DTs where the isentropic slopes are steepest. Figure 2a is a schematic flow pattern reproduced from Namias (1940). This model was also adopted in a textbook by Starr (1942, p. 55):

The moisture emanating from the Gulf of Mexico may flow northward and affect any portion of the continental United States east of the Rocky Mountains... The movement of this moist air is usually in the form of a rather narrow tongue situated above a surface cold front so that the forward portion of the moist outbreak is found in the vicinity of a cyclonic disturbance at the ground...

This description was quoted by Zhu and Newell (1994) to introduce the concept of AR. In fact, this MT model (Fig. 2a) bears an even stronger resemblance to the conceptual model of WCB proposed in Browning (1971) (Fig. 2b).

As compared to the modern AR analysis, the MT model developed in the 1930s had some serious limitations that could have handicapped its effectiveness and chance for success. One is that the isentropic analysis was restricted mainly over continental regions where the

network of upper-air observations must be sufficiently dense. Therefore, offshore moisture transport could not be accurately accommodated. Another disadvantage is that the shape and scale of an MT could vary significantly according to the selected isentropic surfaces. These surfaces should remain in the free atmosphere, because specific humidity may not be considered as a conservative element in the lowest layers where air motion is largely controlled by convection and vertical mixing (Rossby et al. 1937a). It is also difficult to assign exact boundaries to the MTs; the same applied to the WCB analysis, as noticed by Carlson (1980). These problems were eventually addressed and reconciled over time with the development of modern technologies. The current AR analysis has benefited from global upper-air data collected from multiple sources, and methods to identify ARs are often based on the IWV or IVT distributions.

The relationship between MT and AR was further investigated in two case studies using the reanalysis data of 20CRv3. It was demonstrated that an extensive MT on an isentropic chart is often indicative of the presence of an AR. However, some ARs may not be captured well on certain isentropic surfaces. On the other hand, not all MTs on isentropic charts can be identified as an AR based on the IWV or IVT criteria. It was also demonstrated that, while caution must be used in assessing the precipitation intensity and distribution from 20CRv3, this reanalysis dataset offers substantial potential to assess the synoptic features of historic ARs or other high-impact weather events.

As the antecedents for the model of ARs, WCBs or MTs are concerned, I would like to end this article with a quote from an even earlier study of Rossby and Weightman (1926):

The type discussed below, a weak depression from the Northwest slowly approaching the lower Mississippi Valley, and there increasing in intensity under advection of warm, moist air from the Gulf and cold air from Canada, occurs frequently...

**Acknowledgments.** This article originated from a presentation at the Virtual Symposium by the International Atmospheric Rivers Conference Community, 5–9 October 2020 (<https://iarc-symposium.com/>). I would like to thank Anthony Liu, Mindy Brugman, Roxanne Vingarzan, Anna Wilson, Willie Cowan, Jorge Eiras-Barca, and Peter Black for stimulating discussions and suggestions. Dr. Shuzhan Ren conducted an internal review of the first version. Drs. Laura Slivinski and Gilbert Compo (NOAA) are gratefully acknowledged for their invaluable assistance related to the use and interpretation of the 20CRv3 data. ECCC librarians, Alison Dodd and Danny Chan, kindly assisted with manuscript research. Critical and constructive comments from three anonymous reviewers are highly appreciated. Editor Kristine Harper provided many valuable suggestions for improving the final version.

**Data availability statement.** The Twentieth Century Reanalysis V3 data are provided by the NOAA/OAR/ESRL PSL, Boulder, Colorado, from their website at [https://psl.noaa.gov/data/gridded/data.20thC\\_ReanV3.html](https://psl.noaa.gov/data/gridded/data.20thC_ReanV3.html). Daily precipitation data across Canada, the United States, and Mexico in May and September 1936 are downloaded from Climate Data Online, [www.ncdc.noaa.gov/cdo-web/](http://www.ncdc.noaa.gov/cdo-web/), provided by the NOAA's National Centers for Environmental Information.

## References

- Bao, J.-W., S. A. Michelson, P. J. Neiman, F. M. Ralph, and J. M. Wilczak, 2006: Interpretation of enhanced integrated water vapor bands associated with extratropical cyclones: Their formation and connection to tropical moisture. *Mon. Wea. Rev.*, **134**, 1063–1080, <https://doi.org/10.1175/MWR3123.1>.
- Bernard, M., 1940: The application of hydrometeorology to engineering problems. *Proc. Hydraulics Conf.*, Iowa City, IA, University of Iowa, 69–80.
- Bjerknes, V., 1898: Ueber die Bildung von Cirkulationsbewegungen und Wirbeln in reibungslosen Flüssigkeiten. *Vidensk.-Selsk. Skr. Mat.-Naturvidensk. Kl.*, No. 5, 29 pp.
- , 1902: Cirkulation relativ zu der Erde. *Meteor. Z.*, **19**, 97–108.
- Black, A. S., and Coauthors, 2021: Australian northwest cloudbands and their relationship to atmospheric rivers and precipitation. *Mon. Wea. Rev.*, **149**, 1125–1139, <https://doi.org/10.1175/MWR-D-20-0308.1>.
- Bleck, R., 1973: Numerical forecasting experiments based on the conservation of potential vorticity on isentropic surfaces. *J. Appl. Meteor. Climatol.*, **12**, 737–752, [https://doi.org/10.1175/1520-0450\(1973\)012<0737:NFEBOT>2.0.CO;2](https://doi.org/10.1175/1520-0450(1973)012<0737:NFEBOT>2.0.CO;2).
- Brooks, C. F., 1945: Report on the Kansas City meeting, Jan. 24–26, 1945. *Bull. Amer. Meteor. Soc.*, **26**, 33–47, <https://doi.org/10.1175/1520-0477-26.2.33>.
- Browning, K. A., 1971: Radar measurements of air motion near fronts. Part two: Some categories of frontal air motion. *Weather*, **26**, 320–340, <https://doi.org/10.1002/j.1477-8696.1971.tb04211.x>.
- , 1986: Conceptual models of precipitation systems. *Wea. Forecasting*, **1**, 23–41, [https://doi.org/10.1175/1520-0434\(1986\)001<0023:CMOPS>2.0.CO;2](https://doi.org/10.1175/1520-0434(1986)001<0023:CMOPS>2.0.CO;2).
- , 1990: Organization of clouds and precipitation in extratropical cyclones. *Extratropical Cyclones*, C. W. Newton and E. O. Holopainen, Eds., Amer. Meteor. Soc., 129–153, [https://doi.org/10.1007/978-1-944970-33-8\\_8](https://doi.org/10.1007/978-1-944970-33-8_8).
- , 2018: Atmospheric rivers in the U.K. *Bull. Amer. Meteor. Soc.*, **99**, 1108–1109, <https://doi.org/10.1175/BAMS-D-17-0291.1>.
- , and C. W. Pardoe, 1973: Structure of low-level jet streams ahead of mid-latitude cold fronts. *Quart. J. Roy. Meteor. Soc.*, **99**, 619–638, <https://doi.org/10.1002/qj.49709942204>.
- , and F. F. Hill, 1985: Mesoscale analysis of a polar trough interacting with a polar front. *Quart. J. Roy. Meteor. Soc.*, **111**, 445–462, <https://doi.org/10.1002/qj.49711146809>.
- Byers, H. R., 1938: On the thermodynamic interpretation of isentropic charts. *Mon. Wea. Rev.*, **66**, 63–68, [https://doi.org/10.1175/1520-0493\(1938\)66<63:OTTIOL>2.0.CO;2](https://doi.org/10.1175/1520-0493(1938)66<63:OTTIOL>2.0.CO;2).
- , 1960: Carl-Gustaf Arvid Rossby: 1898–1957. *Natl. Acad. Sci.*, **34**, 248–270.
- Carleton, A. M., 1985: Synoptic and satellite aspects of the southwestern U.S. summer ‘monsoon’. *J. Climatol.*, **5**, 389–402, <https://doi.org/10.1002/joc.3370050406>.
- Carlson, T. N., 1980: Airflow through midlatitude cyclones and the comma cloud pattern. *Mon. Wea. Rev.*, **108**, 1498–1509, [https://doi.org/10.1175/1520-0493\(1980\)108<1498:ATMCAT>2.0.CO;2](https://doi.org/10.1175/1520-0493(1980)108<1498:ATMCAT>2.0.CO;2).
- Cerveny, R. S., K. DeBiaise, M. B. Pace, A. W. Ellis, and R. C. Balling Jr., 2011: Reanalysis and extension of Namias’s climatological isentropic analysis: Detection and evaluation of monsoonal, severe storm, drought, and flood events. *Ann. Assoc. Amer. Geogr.*, **101**, 1204–1220, <https://doi.org/10.1080/00045608.2011.584280>.
- Chang, J.-H., 1971: The Chinese monsoon. *Geogr. Rev.*, **61**, 370–395, <https://doi.org/10.2307/213434>.
- Clark, P. A., K. A. Browning, and C. Wang, 2005: The sting at the end of the tail: Model diagnostics of fine-scale three-dimensional structure of the cloud head. *Quart. J. Roy. Meteor. Soc.*, **131**, 2263–2292, <https://doi.org/10.1256/qj.04.36>.
- Compo, G. P., and Coauthors, 2011: The Twentieth Century Reanalysis Project. *Quart. J. Roy. Meteor. Soc.*, **137**, 1–28, <https://doi.org/10.1002/qj.776>.
- Conrad, C. T., 2009: *Severe and Hazardous Weather in Canada: The Geography of Extreme Events*. Oxford University Press, 205 pp.
- Dacre, H. F., P. A. Clark, O. Martinez-Alvarado, M. A. Stringer, and D. A. Lavers, 2015: How do atmospheric rivers form? *Bull. Amer. Meteor. Soc.*, **96**, 1243–1255, <https://doi.org/10.1175/BAMS-D-14-00031.1>.
- Davis, D. D., and Coauthors, 1993: A photostationary state analysis of the NO<sub>2</sub>-NO system based on airborne observations from the subtropical/tropical North and South Atlantic. *J. Geophys. Res.*, **98**, 23 501–23 523, <https://doi.org/10.1029/93JD02412>.
- Davis, M., 1995: Los Angeles after the storm: The dialectic of ordinary disaster. *Antipode*, **27**, 221–241, <https://doi.org/10.1111/j.1467-8330.1995.tb00276.x>.
- Denham, W. S., and D. W. Knoll, 1939: An isentropic analysis of a thunderstorm situation. M.S. thesis, Massachusetts Institute of Technology, 99 pp.
- Dettinger, M., 2004: Fifty-two years of “pineapple-express” storms across the west coast of North America. California Energy Commission Rep. CEC-500-2005-004, 20 pp.
- , F. M. Ralph, and D. A. Lavers, 2015: Setting the stage for a global science of atmospheric rivers. *Eos, Trans. Amer. Geophys. Union*, **96**, <https://doi.org/10.1029/2015EO038675>.
- Du, Y., G. Chen, B. Han, C. Mai, L. Bai, and M. Li, 2020: Convection initiation and growth at the coast of South China. Part I: Effect of the marine boundary layer jet. *Mon. Wea. Rev.*, **148**, 3847–3869, <https://doi.org/10.1175/MWR-D-20-0089.1>.
- Eerme, K., 1996: Greenhouse gases and their impact on the radiation balance. *Estonia in the System of Global Climate Change*, Institute of Ecology, 10–16.
- Environment and Climate Change Canada, 2021: Canada’s top 10 weather stories of 2021. ECCC, [www.canada.ca/en/environment-climate-change/services/top-ten-weather-stories/2021.html](http://www.canada.ca/en/environment-climate-change/services/top-ten-weather-stories/2021.html).
- Espenak, F., and J. Anderson, 1993: Annular solar eclipse of 10 May 1994. National Aeronautics and Space Administration Rep. 1301, 87 pp.
- Fritz, S., 1961: Satellite cloud pictures of a cyclone over the Atlantic Ocean. *Quart. J. Roy. Meteor. Soc.*, **87**, 314–321, <https://doi.org/10.1002/qj.49708737304>.
- Fu, G., S. Liu, X. Li, P. Li, and L. Chen, 2021: Characteristics of atmospheric rivers over the East Asia in middle summers from 2001 to 2016. *J. Ocean Univ. China*, **20**, 235–243, <https://doi.org/10.1007/s11802-021-4513-x>.
- Gimeno, L., R. Nieto, M. Vázquez, and D. A. Lavers, 2014: Atmospheric rivers: A mini-review. *Front. Earth Sci.*, **2**, 2, <https://doi.org/10.3389/feart.2014.00002>.
- , and Coauthors, 2016: Major mechanisms of atmospheric moisture transport and their role in extreme precipitation events. *Annu. Rev. Environ. Resour.*, **41**, 117–141, <https://doi.org/10.1146/annurev-environ-110615-085558>.
- Gorodetskaya, I. V., M. Tsukernik, K. Claes, M. F. Ralph, W. D. Neff, and N. P. M. Van Lipzig, 2014: The role of atmospheric rivers in anomalous snow accumulation in East Antarctica. *Geophys. Res. Lett.*, **41**, 6199–6206, <https://doi.org/10.1002/2014GL060881>.
- Guan, B., and D. E. Waliser, 2019: Tracking atmospheric rivers globally: Spatial distributions and temporal evolution of life cycle characteristics. *J. Geophys. Res. Atmos.*, **124**, 12523–12552, <https://doi.org/10.1029/2019JD031205>.
- , N. P. Molotch, D. E. Waliser, E. J. Fetzer, and P. J. Neiman, 2010: Extreme snowfall events linked to atmospheric rivers and surface air temperature via satellite measurements. *Geophys. Res. Lett.*, **37**, L20401, <https://doi.org/10.1029/2010GL044696>.
- Gyakum, J. R., 2000: Moisture transport to Arctic drainage basins relating to significant precipitation events and cyclogenesis. *The Freshwater Budget of the Arctic Ocean*, E. Lewis et al., Eds., Springer, 197–208.
- Harrold, T. W., 1973: Mechanisms influencing the distribution of precipitation within baroclinic disturbances. *Quart. J. Roy. Meteor. Soc.*, **99**, 232–251, <https://doi.org/10.1002/qj.49709942003>.
- Haynes, B. C., 1940: Meteorology for pilots. U.S. Civil Aeronautics Administration Civil Aeronautics Bulletin 25, 150 pp.
- Hoskins, B. J., M. E. McIntyre, and A. W. Robertson, 1985: On the use and significance of isentropic potential vorticity maps. *Quart. J. Roy. Meteor. Soc.*, **111**, 877–946, <https://doi.org/10.1002/qj.49711147002>.
- Iselin, J. P., and W. J. Gutowski, 1997: Water vapor layers in STORM-FEST rawinsonde observations. *Mon. Wea. Rev.*, **125**, 1954–1963, [https://doi.org/10.1175/1520-0493\(1997\)125<1954:WVLISF>2.0.CO;2](https://doi.org/10.1175/1520-0493(1997)125<1954:WVLISF>2.0.CO;2).

- Iskenderian, H., 1995: A 10-year climatology of Northern Hemisphere tropical cloud plumes and their composite flow patterns. *J. Climate*, **8**, 1630–1637, [https://doi.org/10.1175/1520-0442\(1995\)008<1630:AYCONH>2.0.CO;2](https://doi.org/10.1175/1520-0442(1995)008<1630:AYCONH>2.0.CO;2).
- James, C. N., and R. A. Houze Jr., 2005: Modification of precipitation by coastal orography in storms crossing Northern California. *Mon. Wea. Rev.*, **133**, 3110–3131, <https://doi.org/10.1175/MWR3019.1>.
- Jankov, I., P. J. Schultz, C. J. Anderson, and S. E. Koch, 2007: The impact of different physical parameterizations and their interactions on cold season QPF in the American River basin. *J. Hydrometeorol.*, **8**, 1141–1151, <https://doi.org/10.1175/JHM630.1>.
- Jeong, D., K.-H. Min, G. Lee, and K.-E. Kim, 2014: A case study of mesoscale convective band (MCB) development and evolution along a quasi-stationary front. *Adv. Atmos. Sci.*, **31**, 901–915, <https://doi.org/10.1007/s00376-013-3089-9>.
- Jones, A. H., and C. L. Roe, 1953: The northern Gulf low of February 14, 1953. *Mon. Wea. Rev.*, **81**, 47–52, [https://doi.org/10.1175/1520-0493\(1953\)081<0047:TNGL0F>2.0.CO;2](https://doi.org/10.1175/1520-0493(1953)081<0047:TNGL0F>2.0.CO;2).
- Kaplan, M. L., C. S. Adaniya, P. J. Marzette, K. C. King, S. J. Underwood, and J. M. Lewis, 2009: The role of upstream midtropospheric circulations in the Sierra Nevada enabling leeside (spillover) precipitation. Part II: A secondary atmospheric river accompanying a midlevel jet. *J. Hydrometeorol.*, **10**, 1327–1354, <https://doi.org/10.1175/2009JHM1106.1>.
- Katzfey, J. J., and K. L. McInnes, 1996: GCM simulations of eastern Australian cutoff lows. *J. Climate*, **9**, 2337–2355, [https://doi.org/10.1175/1520-0442\(1996\)009<2337:GSOEAC>2.0.CO;2](https://doi.org/10.1175/1520-0442(1996)009<2337:GSOEAC>2.0.CO;2).
- Kerr, R. A., 2006: Rivers in the sky are flooding the world with tropical waters. *Science*, **313**, 435, <https://doi.org/10.1126/science.313.5786.435>.
- Knarr, A. J., 1941: The Midwest storm of November 11, 1940. *Mon. Wea. Rev.*, **69**, 169–178, [https://doi.org/10.1175/1520-0493\(1941\)069<0169:TMS0N>2.0.CO;2](https://doi.org/10.1175/1520-0493(1941)069<0169:TMS0N>2.0.CO;2).
- Knippertz, P., and J. E. Martin, 2007: A Pacific moisture conveyor belt and its relationship to a significant precipitation event in the semiarid southwestern United States. *Wea. Forecasting*, **22**, 125–144, <https://doi.org/10.1175/WAF963.1>.
- , and H. Wernli, 2010: A Lagrangian climatology of tropical moisture exports to the Northern Hemispheric extratropics. *J. Climate*, **23**, 987–1003, <https://doi.org/10.1175/2009JCLI3333.1>.
- Kuhnel, I., 1989: Tropical-extratropical cloudband climatology based on satellite data. *Int. J. Climatol.*, **9**, 441–463, <https://doi.org/10.1002/joc.3370090502>.
- Lackmann, G. M., and J. R. Gyakum, 1999: Heavy cold-season precipitation in the northwestern United States: Synoptic climatology and an analysis of the flood of 17–18 January 1986. *Wea. Forecasting*, **14**, 687–700, [https://doi.org/10.1175/1520-0434\(1999\)014<0687:HCS0PIT>2.0.CO;2](https://doi.org/10.1175/1520-0434(1999)014<0687:HCS0PIT>2.0.CO;2).
- Lau, K.-M., H.-T. Wu, and S. Yang, 1998: Hydrologic processes associated with the first transition of the Asian summer monsoon: A pilot satellite study. *Bull. Amer. Meteor. Soc.*, **79**, 1871–1882, [https://doi.org/10.1175/1520-0477\(1998\)079<1871:HPAWTF>2.0.CO;2](https://doi.org/10.1175/1520-0477(1998)079<1871:HPAWTF>2.0.CO;2).
- Lavers, D. A., R. P. Allan, E. F. Wood, G. Villarini, D. J. Brayshaw, and A. J. Wade, 2011: Winter floods in Britain are connected to atmospheric rivers. *Geophys. Res. Lett.*, **38**, L23803, <https://doi.org/10.1029/2011GL049783>.
- , G. Villarini, R. P. Allan, E. F. Wood, and A. J. Wade, 2012: The detection of atmospheric rivers in atmospheric reanalyses and their links to British winter floods and the large-scale climatic circulation. *J. Geophys. Res.*, **117**, D20106, <https://doi.org/10.1029/2012JD018027>.
- Leese, J. A., 1962: The role of advection in the formation of vortex cloud patterns. *Tellus*, **14**, 409–421, <https://doi.org/10.3402/tellusa.v14i4.9568>.
- Loukas, A., and M. C. Quick, 1996: Spatial and temporal distribution of storm precipitation in southwestern British Columbia. *J. Hydrol.*, **174**, 37–56, [https://doi.org/10.1016/0022-1694\(95\)02754-8](https://doi.org/10.1016/0022-1694(95)02754-8).
- Mahoney, K., and Coauthors, 2016: Understanding the role of atmospheric rivers in heavy precipitation in the southeast United States. *Mon. Wea. Rev.*, **144**, 1617–1632, <https://doi.org/10.1175/MWR-D-15-0279.1>.
- Martínez-Alvarado, O., H. Joos, J. Chagnon, M. Boettcher, S. Gray, R. Plant, J. Methven, and H. Wernli, 2014: The dichotomous structure of the warm conveyor belt. *Quart. J. Roy. Meteor. Soc.*, **140**, 1809–1824, <https://doi.org/10.1002/qj.2276>.
- McGuirk, J. P., and D. J. Ulsh, 1990: Evolution of tropical plumes in VAS water vapor imagery. *Mon. Wea. Rev.*, **118**, 1758–1766, [https://doi.org/10.1175/1520-0493\(1990\)118<1758:EOTPIV>2.0.CO;2](https://doi.org/10.1175/1520-0493(1990)118<1758:EOTPIV>2.0.CO;2).
- , A. H. Thompson, and N. R. Smith, 1987: Moisture bursts over the tropical Pacific Ocean. *Mon. Wea. Rev.*, **115**, 787–798, [https://doi.org/10.1175/1520-0493\(1987\)115<0787:MBOTTP>2.0.CO;2](https://doi.org/10.1175/1520-0493(1987)115<0787:MBOTTP>2.0.CO;2).
- , —, and J. R. Schaefer, 1988: An eastern Pacific tropical plume. *Mon. Wea. Rev.*, **116**, 2505–2521, [https://doi.org/10.1175/1520-0493\(1988\)116<2505:AEPTP>2.0.CO;2](https://doi.org/10.1175/1520-0493(1988)116<2505:AEPTP>2.0.CO;2).
- Means, L. L., 1944: The nocturnal maximum occurrence of thunderstorms in the midwestern states. University of Chicago Dept. of Meteorology Misc. Rep. 16, 38 pp., [www.flame.org/~cdoswell/publications/Means\\_44.pdf](http://www.flame.org/~cdoswell/publications/Means_44.pdf).
- Miller, J. A., 1973: Picture of the month: Dry air intrusion into a low-level moist tongue as viewed by ATS 3. *Mon. Wea. Rev.*, **101**, 594–595, [https://doi.org/10.1175/1520-0493\(1973\)101<0594:POTMDA>2.3.CO;2](https://doi.org/10.1175/1520-0493(1973)101<0594:POTMDA>2.3.CO;2).
- Mills, G. A., 1989: Dynamics of a rapid cloud band development over southeastern Australia. *Mon. Wea. Rev.*, **117**, 1402–1422, [https://doi.org/10.1175/1520-0493\(1989\)117<1402:DOARCB>2.0.CO;2](https://doi.org/10.1175/1520-0493(1989)117<1402:DOARCB>2.0.CO;2).
- Mitchell, C. L., and H. Wexler, 1941: How the daily forecast is made. *Climate and Man: Yearbook of Agriculture*, U.S. Dept. of Agriculture, 579–598.
- Mo, R., 2016: Atmospheric rivers in the Northeast Pacific: Pineapple express. *Meteorology Today: An Introduction to Weather, Climate, and the Environment*, 2nd ed. C. D. Ahrens, P. L. Jackson, and C. E. O. Jackson, Eds., Nelson Education Ltd., 360–361.
- , and H. Lin, 2019: Tropical–mid-latitude interactions: Case study of an inland-penetrating atmospheric river during a major winter storm over North America. *Atmos.–Ocean*, **57**, 208–232, <https://doi.org/10.1080/07055900.2019.1617673>.
- , M. M. Brugman, J. A. Milbrandt, J. Goosen, Q. Geng, C. Emond, J. Bau, and A. Erfani, 2019: Impacts of hydrometeor drift on orographic precipitation: Two case studies of landfalling atmospheric rivers in British Columbia, Canada. *Wea. Forecasting*, **34**, 1211–1237, <https://doi.org/10.1175/WAF-D-18-0176.1>.
- , R. So, M. M. Brugman, C. Mooney, A. Q. Liu, M. Jakob, A. Castellan, and R. Vingarzan, 2021: Column relative humidity and primary condensation rate as two useful supplements to atmospheric river analysis. *Water Resour. Res.*, **57**, e2021WR029678, <https://doi.org/10.1029/2021WR029678>.
- Moore, B. J., P. J. Neiman, F. M. Ralph, and F. E. Barthold, 2012: Physical processes associated with heavy flooding rainfall in Nashville, Tennessee, and vicinity during 1–2 May 2010: The role of an atmospheric river and mesoscale convective systems. *Mon. Wea. Rev.*, **140**, 358–378, <https://doi.org/10.1175/MWR-D-11-00126.1>.
- , K. M. Mahoney, E. M. Sukovich, R. Cifelli, and T. M. Hamill, 2015: Climatology and environmental characteristics of extreme precipitation events in the southeastern United States. *Mon. Wea. Rev.*, **143**, 718–741, <https://doi.org/10.1175/MWR-D-14-00065.1>.
- Namias, J., 1938: Thunderstorm forecasting with the aid of isentropic charts. *Bull. Amer. Meteor. Soc.*, **19**, 1–14, <https://doi.org/10.1175/1520-0477-19.1.1>.
- , 1939a: Two important factors controlling winter-time precipitation in the southeastern United States. *Eos, Trans. Amer. Geophys. Union*, **20**, 341–348, <https://doi.org/10.1029/TR020i003p00341-2>.
- , 1939b: The use of isentropic analysis in short term forecasting. *J. Aeronaut. Sci.*, **6**, 295–298, <https://doi.org/10.2514/8.860>.
- , 1940: Isentropic analysis. *Weather Analysis and Forecasting: A Textbook on Synoptic Meteorology*, S. Petterssen, Ed., McGraw-Hill, 351–377.
- , 1955: Some meteorological aspects of drought: With special reference to the summers of 1952–54 over the United States. *Mon. Wea. Rev.*, **83**, 199–205, [https://doi.org/10.1175/1520-0493\(1955\)083<0199:SMAOD>2.0.CO;2](https://doi.org/10.1175/1520-0493(1955)083<0199:SMAOD>2.0.CO;2).
- , and A. J. Wagner, 1971: Warm continental anticyclone with peripheral moist tongues: A recent example illustrated by satellite photographs. *Mon. Wea. Rev.*, **99**, 162–164, [https://doi.org/10.1175/1520-0493\(1971\)099<0162:WCAWPM>2.3.CO;2](https://doi.org/10.1175/1520-0493(1971)099<0162:WCAWPM>2.3.CO;2).

- Neiman, P. J., F. M. Ralph, G. A. Wick, Y.-H. Kuo, T.-K. Wee, Z. Ma, G. H. Taylor, and M. D. Dettinger, 2008a: Diagnosis of an intense atmospheric river impacting the Pacific Northwest: Storm summary and offshore vertical structure observed with COSMIC satellite retrievals. *Mon. Wea. Rev.*, **136**, 4398–4420, <https://doi.org/10.1175/2008MWR2550.1>.
- , —, —, J. D. Lundquist, and M. D. Dettinger, 2008b: Meteorological characteristics and overland precipitation impacts of atmospheric rivers affecting the west coast of North America based on eight years of SSM/I satellite observations. *J. Hydrometeor.*, **9**, 22–47, <https://doi.org/10.1175/2007JHM855.1>.
- Newell, R. E., N. E. Newell, Y. Zhu, and C. Scott, 1992: Tropospheric rivers? A pilot study. *Geophys. Res. Lett.*, **19**, 2401–2404, <https://doi.org/10.1029/92GL02916>.
- Osmun, J. W. W., 1937: An introductory discussion of the isentropic chart. Weather Bureau Tech. Rep., 16 pp., <https://ia801004.us.archive.org/29/items/CAT31050414/CAT31050414.pdf>.
- Paltan, H., D. Waliser, W. H. Lim, B. Guan, D. Yamazaki, R. Pant, and S. Dadson, 2017: Global floods and water availability driven by atmospheric rivers. *Geophys. Res. Lett.*, **44**, 10387–10395, <https://doi.org/10.1002/2017GL074882>.
- Petterssen, S., 1940: *Weather Analysis and Forecast: A Textbook on Synoptic Meteorology*. McGraw-Hill, 503 pp.
- Pryne, E., and K. Long, 1991: Trouble in the paradise—Homes built in path of flood peril. *Seattle Times*, 10 February, <https://archive.seattletimes.com/archive/?date=19910210&slug=1265476>.
- Ralph, F. M., P. J. Neiman, and G. A. Wick, 2004: Satellite and CALJET aircraft observations of atmospheric rivers over the eastern North Pacific Ocean during the winter of 1997/98. *Mon. Wea. Rev.*, **132**, 1721–1745, [https://doi.org/10.1175/1520-0493\(2004\)132<1721:SACAOO>2.0.CO;2](https://doi.org/10.1175/1520-0493(2004)132<1721:SACAOO>2.0.CO;2).
- , —, and R. Rotunno, 2005: Dropsonde observations in low-level jets over the northeastern Pacific Ocean from CALJET-1998 and PACJET-2001: Mean vertical-profile and atmospheric-river characteristics. *Mon. Wea. Rev.*, **133**, 889–910, <https://doi.org/10.1175/MWR2896.1>.
- , —, G. A. Wick, S. I. Gutman, M. D. Dettinger, D. R. Cayan, and A. B. White, 2006: Flooding on California's Russian River: Role of atmospheric rivers. *Geophys. Res. Lett.*, **33**, L13801, <https://doi.org/10.1029/2006GL026689>.
- , and Coauthors, 2017a: Atmospheric rivers emerge as a global science and applications focus. *Bull. Amer. Meteor. Soc.*, **98**, 1969–1973, <https://doi.org/10.1175/BAMS-D-16-0262.1>.
- , and Coauthors, 2017b: Dropsonde observations of total integrated water vapor transport within North Pacific atmospheric rivers. *J. Hydrometeor.*, **18**, 2577–2596, <https://doi.org/10.1175/JHM-D-17-0036.1>.
- , M. D. Dettinger, M. M. Cairns, T. J. Galarneau, and J. Eylander, 2018: Defining “atmospheric river”: How the Glossary of Meteorology helped resolve a debate. *Bull. Amer. Meteor. Soc.*, **99**, 837–839, <https://doi.org/10.1175/BAMS-D-17-0157.1>.
- , —, L. J. Schick, and M. L. Anderson, 2020: Introduction to atmospheric rivers. *Atmospheric Rivers*, F. M. Ralph et al., Eds., Springer, 1–13, [https://doi.org/10.1007/978-3-030-28906-5\\_1](https://doi.org/10.1007/978-3-030-28906-5_1).
- Rosby, C.-G., 1932: Thermodynamics applied to air mass analysis. *Meteorological Papers*, Vol. I, No. 3, Massachusetts Institute of Technology, 41 pp., <https://doi.org/10.1575/1912/1139>.
- , 1939: On the role of isentropic mixing in the general circulation of the atmosphere. *Proc. Fifth Int. Congress on Theoretical and Applied Mechanics*, Cambridge, MA, IUTAM, 373–378.
- , 1940: Planetary flow patterns in the atmosphere. *Quart. J. Roy. Meteor. Soc.*, **66**, 68–87.
- , 1941: The scientific basis of modern meteorology. *Climate and Man: Yearbook of Agriculture*, U.S. Dept. of Agriculture, 599–655.
- , and R. H. Weightman, 1926: Application of the polar-front theory to a series of American weather maps. *Mon. Wea. Rev.*, **54**, 485–496, [https://doi.org/10.1175/1520-0493\(1926\)54<485:AOTPTT>2.0.CO;2](https://doi.org/10.1175/1520-0493(1926)54<485:AOTPTT>2.0.CO;2).
- , and Coauthors, 1937a: Aerological evidence of large-scale mixing in the atmosphere. *Eos, Trans. Amer. Geophys. Union*, **18**, 130–136, <https://doi.org/10.1029/TR018i001p00130-2>.
- , and Coauthors, 1937b: Isentropic analysis. *Bull. Amer. Meteor. Soc.*, **18**, 201–209, <https://doi.org/10.1175/1520-0477-18.6-7.201>.
- , J. Namias, and R. G. Simmers, 1938: Fluid mechanics applied to the study of atmospheric circulations. Part I: A study of flow patterns with the aid of isentropic analysis. Massachusetts Institute of Technology–Woods Hole Oceanographic Institution Paper in Physical Oceanography and Meteorology 7, 125 pp., <https://doi.org/10.1575/1912/1096>.
- , and Coauthors, 1939: Relation between variations in the intensity of the zonal circulation of the atmosphere and the displacements of the semi-permanent centers of action. *J. Mar. Res.*, **2**, 38–55, <https://doi.org/10.1357/002224039806649023>.
- Rutz, J. J., W. J. Steenburgh, and F. M. Ralph, 2014: Climatological characteristics of atmospheric rivers and their inland penetration over the western United States. *Mon. Wea. Rev.*, **142**, 905–921, <https://doi.org/10.1175/MWR-D-13-00168.1>.
- Saito, N., 1966: A preliminary study of the summer monsoon of southern and eastern Asia. *J. Meteor. Soc. Japan*, **44**, 44–59, [https://doi.org/10.2151/jmsj1965.44.1\\_44](https://doi.org/10.2151/jmsj1965.44.1_44).
- Semonin, R. G., 1960: Artificial precipitation potential during dry periods in Illinois. *Physics of Precipitation: Proc. Cloud Physics Conf.*, Woods Hole, MA, Amer. Geophys. Union, 424–431.
- Shaw, N., 1929: Distribution of temperature in the first 25 kilometres over the Earth. *Nature*, **123**, 906, <https://doi.org/10.1038/123906a0>.
- , 1930: *The Physical Processes of Weather. Vol. III, Manual of Meteorology*, Cambridge University Press, 445 pp.
- Shields, C. A., and Coauthors, 2018: Atmospheric River Tracking Method Inter-comparison Project (ARTMIP): Project goals and experimental design. *Geosci. Model Dev.*, **11**, 2455–2474, <https://doi.org/10.5194/gmd-11-2455-2018>.
- Showalter, A. K., 1944: An approach to quantitative forecasting of precipitation. *Bull. Amer. Meteor. Soc.*, **25**, 137–142, <https://doi.org/10.1175/1520-0477-25.4.137>.
- , and S. B. Solot, 1942: Computation of maximum possible precipitation. *Eos, Trans. Amer. Geophys. Union*, **23**, 258–274, <https://doi.org/10.1029/TR023i002p00258>.
- Slivinski, L. C., and Coauthors, 2019: Towards a more reliable historical reanalysis: Improvements for version 3 of the Twentieth Century Reanalysis system. *Quart. J. Roy. Meteor. Soc.*, **145**, 2876–2908, <https://doi.org/10.1002/qj.3598>.
- , and Coauthors, 2021: An evaluation of the performance of the Twentieth Century Reanalysis version 3. *J. Climate*, **34**, 1417–1438, <https://doi.org/10.1175/JCLI-D-20-0505.1>.
- Smirnov, V. V., and G. W. K. Moore, 1999: Spatial and temporal structure of atmospheric water vapor transport in the Mackenzie River basin. *J. Climate*, **12**, 681–696, [https://doi.org/10.1175/1520-0442\(1999\)012<0681:SATSOA>2.0.CO;2](https://doi.org/10.1175/1520-0442(1999)012<0681:SATSOA>2.0.CO;2).
- , and —, 2001: Short-term and seasonal variability of the atmospheric water vapor transport through the Mackenzie River basin. *J. Hydrometeor.*, **2**, 441–452, [https://doi.org/10.1175/1525-7541\(2001\)002<0441:STASVO>2.0.CO;2](https://doi.org/10.1175/1525-7541(2001)002<0441:STASVO>2.0.CO;2).
- Sodemann, H., and A. Stohl, 2013: Moisture origin and meridional transport in atmospheric rivers and their association with multiple cyclones. *Mon. Wea. Rev.*, **141**, 2850–2868, <https://doi.org/10.1175/MWR-D-12-00256.1>.
- Starr, V. P., 1942: *Basic Principles of Weather Forecasting*. Harper and Brothers, 299 pp.
- Stewart, R. E., and S. R. Macpherson, 1989: Winter storm structure and melting-induced circulations. *Atmos.–Ocean*, **27**, 5–23, <https://doi.org/10.1080/07055900.1989.9649326>.
- Swenson, B., 1940: River stages and floods. *Mon. Wea. Rev.*, **68**, 258–262, [https://doi.org/10.1175/1520-0493\(1940\)068<0258:RSAF>2.0.CO;2](https://doi.org/10.1175/1520-0493(1940)068<0258:RSAF>2.0.CO;2).
- Takahashi, K., T. Asakura, M. Hirose, M. Iida, and N. Nakamura, 1954: Analysis of extraordinarily heavy rains at the end of bai-u, one of the rainy season in Japan. *J. Meteor. Soc. Japan*, **32**, 281–289, [https://doi.org/10.2151/jmsj1923.32.9-10\\_281](https://doi.org/10.2151/jmsj1923.32.9-10_281).
- Tan, Y., F. Zwiers, S. Yang, C. Li, and K. Deng, 2020: The role of circulation and its changes in present and future atmospheric rivers over western North America. *J. Climate*, **33**, 1261–1281, <https://doi.org/10.1175/JCLI-D-19-0134.1>.
- Waters, S. D., 1993: Storm report: January 1993. Flood Control District of Maricopa County Tech. Rep., 81 pp., [https://alert.fcd.maricopa.gov/alert/01XX93/report\\_0193.pdf](https://alert.fcd.maricopa.gov/alert/01XX93/report_0193.pdf).

- Waugh, D. W., 2005: Impact of potential vorticity intrusions on subtropical upper tropospheric humidity. *J. Geophys. Res.*, **110**, D11305, <https://doi.org/10.1029/2004JD005664>.
- Weightman, R. H., 1939: Progress in applying new synoptic aids to day-to-day forecasting. *Bull. Amer. Meteor. Soc.*, **20**, 169–177, <https://doi.org/10.1175/1520-0477-20.4.169>.
- , 1940: *Forecasting from Synoptic Weather Charts*. U.S. Dept. of Agriculture, 52 pp.
- Wernli, H., 1997: A Lagrangian-based analysis of extratropical cyclones. II: A detailed case-study. *Quart. J. Roy. Meteor. Soc.*, **123**, 1677–1706, <https://doi.org/10.1002/qj.49712354211>.
- , and H. C. Davies, 1997: A Lagrangian-based analysis of extratropical cyclones. I: The method and some applications. *Quart. J. Roy. Meteor. Soc.*, **123**, 467–489, <https://doi.org/10.1002/qj.49712353811>.
- Wexler, H., and J. Namias, 1938: Mean monthly isentropic charts and their relation to departures of summer rainfall. *Eos, Trans. Amer. Geophys. Union*, **19**, 164–170, <https://doi.org/10.1029/TR019i001p00164>.
- Willett, H. C., R. A. Allen, and J. Namias, 1941: Report of the five-day forecasting procedure, verification and research as conducted between July 1940 and August 1941. Massachusetts Institute of Technology–Woods Hole Oceanographic Institution Paper in Physical Oceanography and Meteorology 9, 88 pp., <https://doi.org/10.1575/1912/1052>.
- Wood, C., 1998: A Trudeau tragedy. *Macleans*, Vol. 23, No. 11, 82.
- Ye, C., H. Zhang, A. Moise, and R. Mo, 2020: Atmospheric rivers in the Australia-Asian region: A BoM-CMA collaborative study. *J. South. Hemisphere Earth Syst. Sci.*, **70**, 3–16, <https://doi.org/10.1071/ES19025>.
- Zhou, Y., H. Kim, and B. Guan, 2018: Life cycle of atmospheric rivers: Identification and climatological characteristics. *J. Geophys. Res. Atmos.*, **123**, 12–715, <https://doi.org/10.1029/2018JD029180>.
- Zhu, Y., and R. E. Newell, 1994: Atmospheric rivers and bombs. *Geophys. Res. Lett.*, **21**, 1999–2002, <https://doi.org/10.1029/94GL01710>.
- , and —, 1998: A proposed algorithm for moisture fluxes from atmospheric rivers. *Mon. Wea. Rev.*, **126**, 725–735, [https://doi.org/10.1175/1520-0493\(1998\)126<0725:APAFMF>2.0.CO;2](https://doi.org/10.1175/1520-0493(1998)126<0725:APAFMF>2.0.CO;2).